LAURO SOLIA

GREEN AMMONIA SUPPLY CHAIN OPTIMIZATION FOR THE STATE OF MATO GROSSO: A MIXED-INTEGER NONLINEAR PROGRAMMING APPROACH

São Paulo
2025

LAURO SOLIA

GREEN AMMONIA SUPPLY CHAIN OPTIMIZATION FOR THE STATE OF MATO GROSSO: A MIXED-INTEGER NONLINEAR PROGRAMMING APPROACH

Graduation Work presented to the Escola Politécnica - University of São Paulo for attaining the Bachelor's Degree in Production Engineering.

Advisor:

Prof. Dr. Celma de Oliveira Ribeiro

São Paulo
2025

Ad maiorem Dei gloriam

ACKNOWLEDGMENTS

I would like to express my deepest gratitude to my advisor, Prof. Dr. Celma de Oliveira Ribeiro, for her invaluable guidance throughout much of my academic journey, especially in regards to this work. I have to appreciate the sacrifices she makes to help her students, always being available to provide all the support needed for our work to bear fruit. I also want to extend my thanks to others that contributed directly to this work, namely Prof. Dr. Erik Rego and Prof. Dr. Cláudio Oller, for their insightful comments and suggestions that helped improve the quality of this work, as well as Dr. Raphael Dutenkefer who kindly provided me with data from an unpublished research project he conducted.

To God, I must say that I am absolutely grateful to be included in His plans, as every other person is, and even more grateful for the joy of playing my part in them gleefully, sustained by the knowledge of His love and mercy, which is always before me, especially when I behold a crucifix.

To my parents, I owe the opportunity to not only be, but to be able to study and pursue my dreams. Their unconditional support and encouragement have been a perfect demonstration of love, which is the best gift one can receive. I extend this gratitude to the rest of my family, close and distant, hodiernal and ancestral, for all the values and teachings that have shaped me into the person I am today.

Finally, to my friends, both old and new, I want to express my appreciation for their companionship and support throughout this journey. Their presence has made this experience more enjoyable and memorable.

ABSTRACT

Ammonia consumption for fertilizer applications in Brazil has increased sharply in recent years, reinforcing the country's dependence on imports and exposing its agricultural sector to price volatility and supply-chain risks. At the same time, the National Plan of Fertilizers explicitly encourages the integration of green hydrogen and green ammonia into the fertilizer chain. In this context, this work investigates the economic viability of producing green ammonia in a decentralized way in Brazil, focusing on the state of Mato Grosso, the country's leading producer of nitrogen-intensive crops and a region with high solar potential.

A mixed-integer non-linear programming (MINLP) model is proposed to decide on the location and sizing of multiple green ammonia plants designed to meet the entire fertilizer-related ammonia demand of Mato Grosso over a multi-decade horizon, while minimizing the Levelized Cost of Ammonia (LCOA). The model represents the main steps of a green ammonia supply chain, i.e., renewable electricity generation, water electrolysis, membrane air separation, the Haber-Bosch synthesis loop, and the distribution of ammonia and by-product oxygen between municipalities, and is evaluated under two plant-sizing regimes ("Small Plant" and "Medium Plant") and multiple demand and parameter scenarios.

For the baseline "avg" demand scenario and central values of the discount rate and economies of scale exponent, the optimal configurations concentrate plants around the main demand hubs, especially Sorriso and neighbouring municipalities. The more centralized "Medium Plant" regime achieves a system LCOA of 602.80 US$/tonne, while the more distributed "Small Plant" regime yields 656.85 US$/tonne, an increase of about 9%. Sensitivity analyses indicate that the discount rate and economies of scale parameter are the dominant drivers of LCOA variation between the parameters studied, whereas logistics costs and demand spatial distribution have comparatively minor effects. Across all cases, the revenue from selling by-product oxygen reduces LCOA by roughly 5 US$/tonne but does not change the qualitative conclusions.

Overall, the results suggest that decentralized green ammonia production in Mato Grosso is economically plausible within certain parameter ranges, but its viability is strongly contingent on financing conditions and the realization of economies of scale. The modeling framework developed here provides a basis for extending the analysis to the national scale and for supporting public and private decisions related to the implementation of the Brazilian National Plan of Fertilizers.

Keywords: green ammonia; green hydrogen; fertilizer supply chain; location-allocation; mixed-integer nonlinear programming; levelized cost of ammonia; Brazil; Mato Grosso.

LIST OF FIGURES

LIST OF TABLES

CONTENTS

1 INTRODUCTION

According to IBGE (2023), ammonia consumption in Brazil specifically for fertilizers has rapidly increased in recent years, nearly tripling from 2020 to 2022. This growth is primarily attributed to an increase in domestic production, although imports have also risen. This molecule holds particular significance for the agricultural sector, being a fundamental component in nitrogen fertilizer production. Moreover, ammonia has demonstrated potential viability as an energy carrier within a decarbonized energy system, as highlighted by WAN et al. (2021).

The literature on green ammonia production in Brazil remains limited, as most studies highlight only the country's potential to produce it without providing detailed data on plant construction, maintenance and logistics costs, which is the case of LAGARINHOS; AZEVEDO (2024). Additionally, SANTOS et al. (2025) and NADALETI et al. (2023) specifically examine the potential for producing green ammonia using distinct biomass sources.

The government of Brazil, through its Ministry of Industry, Foreign Trade and Services, has published a national fertilizer plan (2023), in which it states as the 22nd goal (in free translation):

"Creation of market development mechanisms by stimulating the diversification of raw materials ('feedstocks') for the production of nitrogen fertilizers, connected to the green hydrogen and biomethane chain, considering a plan to add 5% by mass of 'green ammonia equivalent' per year from 2027 and reaching 20% in 2030."

The four actions associated with it are, also in free translation:

- "Action 130 - Attracting investments for the installation of nitrogen plants based on green/blue ammonia";
- "Action 131 - Integration of the National Natural Gas and Hydrogen Policy with the fertilizer chain in Brazil";
- "Action 132 - Promoting technological development for the implementation of nitrogen plants based on green/blue hydrogen";

- “Action 133 - Integration of the fertilizer chain with energy solutions taking advantage of the potential for clean energy generation (wind/solar potential) for the production of green hydrogen/ammonia, via electrolysis routes (or related processes)”.

From this, one can observe a clear governmental commitment to promoting the sustainable production of ammonia in Brazil, primarily to supply the country’s expanding agricultural sector with nitrogen-based fertilizers. The low-carbon profile of green ammonia, together with the possibility of local production using Brazil’s abundant renewable energy resources, makes it a promising alternative to conventional ammonia production methods that rely on fossil fuels and require transport over long distances.

For example, supplying the growing corn production in Sorriso - MT with imported ammonia (or already produced nitrogen fertilizers) entails maritime transportation to Brazilian ports, followed by approximately 1970 kilometers of road transportation between Santos - SP and Sorriso - MT[1]. This dependence also leaves Brazilian agriculture vulnerable to fluctuations in international fertilizer prices and to supply-chain disruptions, which can be interpreted as a national security issue.

This study closely aligns with the objectives outlined in the national plan by providing an in-depth analysis of the costs associated with producing green ammonia in Brazil in a decentralized manner. The study proposes a mixed-integer non-linear programming (MINLP) model to determine the location and sizing of multiple green ammonia plants to supply the entire demand for nitrogen fertilizers in the state of Mato Grosso while minimizing the Levelized Cost of Ammonia (LCOA). The LCOA is a widely used metric to evaluate the economic feasibility of ammonia production projects, given that it accounts for all costs over the project lifetime and divides them by the total amount of ammonia produced, with both quantities discounted to present value. This approach enables a comprehensive evaluation and modeling of the different cost components involved in the production and distribution of green ammonia, as detailed in Chapter 3. In applying this framework, a trade-off is expected between economies of scale in plant size and transportation costs from plants to demand sites.

The choice of Mato Grosso as the study area is justified by its status as Brazil’s leading producer of corn and other nitrogen-intensive crops, as well as by its high solar potential, which is crucial for producing green hydrogen via electrolysis. If this case study indicates that a decentralized production model is economically viable, a significant next step would be to expand the scope to the entire country, given that demand for nitrogen fertilizers is growing across all

[1]This route is only used as an example, so it is not necessarily the best route, since the use of river ports in the Northern region can be more cost effective

regions and that this decentralized pattern of fertilizer consumption is also observed at the national scale. Because the study incorporates the temporal dimension of supply-chain costs, it includes a forecast of ammonia demand in the state based on publicly available, municipality-level historical data.

The main objective of this work is to assess whether decentralized green ammonia production is economically viable, addressed through three specific research questions:

- What are the optimal sizes and locations of green ammonia plants to supply the nitrogen-fertilizer demand in Mato Grosso, considering the trade-off between economies of scale and transportation costs?
- What is the impact of enforcing a distributed production system by limiting the maximum plant size and the number of plants per municipality on the Levelized Cost of Ammonia (LCOA)?
- How sensitive is the LCOA to variations in hard-to-estimate parameters such as ammonia demand, economies of scale, and logistics costs?

To answer these questions, the study is structured as follows. Chapter 2 reviews the existing literature on relevant topics, including clean energy, ammonia production, economic evaluation tools, and a survey of optimization tools for supply-chain modeling. Chapter 3 details the methodology employed, including the mathematical model, data sources, the assumptions made, and the solution approach. Chapter 4 presents the results obtained from the model, including sensitivity analyses and a discussion of the findings. Finally, Chapter 5 concludes the study by summarizing the main findings, discussing their implications, and suggesting directions for future research.

2 LITERATURE REVIEW

2.1 Hydrogen

Hydrogen has been extensively studied over the past two decades, particularly within the context of energy system decarbonization. This interest arises because hydrogen can be produced at any location with access to water and electricity, and, when generated using renewable energy sources, it can be classified as a clean energy carrier (YUE et al., 2021).

NICOLETTI et al. (2015) compared hydrogen to traditional carbon-based fuels and concluded that hydrogen is significantly superior as a fuel or energy carrier from an environmental standpoint (assuming water vapor is either non-polluting or effectively captured). However, despite hydrogen having a specific energy by mass three times greater than gasoline, numerous practical challenges remain regarding its utilization, particularly in storage and distribution, due to its low volumetric energy density. To address these challenges, KLERKE et al. (2008) proposed ammonia as a viable hydrogen carrier, which subsequently attracted considerable attention in the following years. A more recent study by WAN et al. (2021) also emphasized ammonia as a key resource for enabling a sustainable, hydrogen-based economy. Alternative solutions have similarly been explored in the literature; for instance, PREUSTER; PAPP; WASSERSCHEID (2017) investigated Liquid Organic Hydrogen Carriers (LOHCs). Table 2.1 presents a comparative overview of key attributes for these various solutions.

Table 2.1: properties of Hydrogen Carriers

Carrier	**H_2 content**	**Storage T (∘C)/P (bar)**	**Gravimetric energy density(MJ kg^{-1})**	**Volumetric energy density(GJ m^{-3})**	**Reference**

Continued on next page

Table 2.1 – continued from previous page

Carrier	**H_2 content**	**Storage T (∘C)/P (bar)**	**Gravimetric energy density(MJ kg^{-1})**	**Volumetric energy density(GJ m^{-3})**	**Reference**
Hydrogen	100%	20/250	120.21	2.15	(WAN et al., 2021)
Ammonia	17.6%	20/10	18.65	11.38	(WAN et al., 2021)
LOHC (MCH/toluene)	6.2%	20/1	7.15[1]	5.5	(PANIGRAHI et al., 2024)

Source: Author.

Figure 2.1 shows many ways to synthesize hydrogen and the following sections will deepen the discussion on the most relevant methods for this work.

Figure 2.1: Various Hydrogen Production Methods

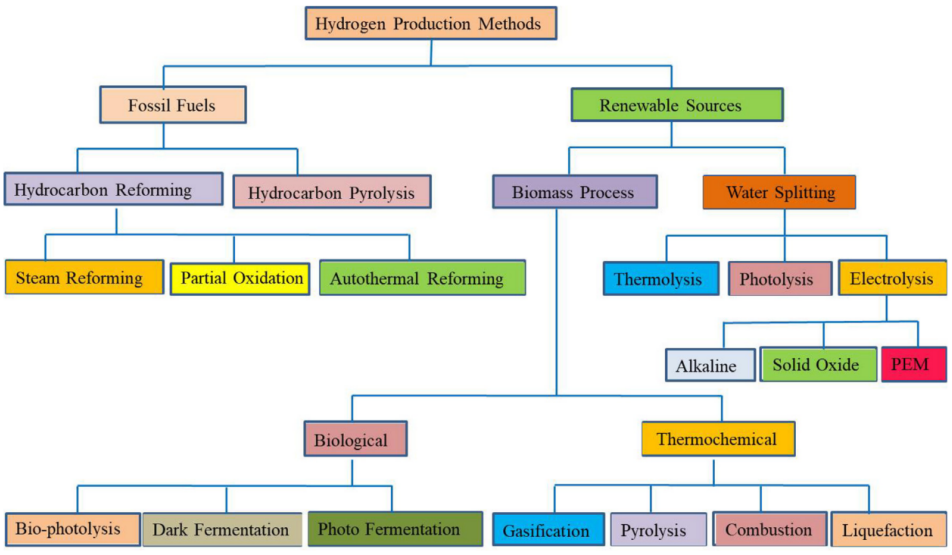

Source: KUMAR; HIMABINDU (2019).

[1]Gravimetric energy density of LOHC (MCH/toluene) can be calculated using its density of 769 kg m^{-3} provided by (WIJAYANTA et al., 2019) and the result is: 7.15 MJ kg^{-1}

2.1.1 Hydrogen "Colours"

Hydrogen is commonly classified according to its environmental impact and production method. Table 2.2 presents the different hydrogen "colours", as described in HERMESMANN; MüLLER (2022).

Table 2.2: Hydrogen colours

Associated Colour	**"Grey"**	**"Blue"**	**"Turquoise"**	**"Green"**
Primary Feedstock	Natural gas	Natural gas	Natural gas	Water
Production Technology	Steam methane reforming (SMR)	SMR with carbon capture & storage (CCS)	Methane pyrolysis (MP)	Polymer electrolyte membrane water Electrolysis (PEMEL)
Technology readiness level (TRL)	Commercial (TRL 9)	Industrial scale (TRL 8-9)	Research & development (TRL 3-4)	Commercial (TRL 9)
Process-related CO_2 emissions	High-CO_2	Low-CO_2	CO_2-free	Carbon free

Source: HERMESMANN; MüLLER (2022).

2.1.1.1 Grey Hydrogen

According to HERMESMANN; MüLLER (2022), grey hydrogen can be produced through various methods, such as partial oxidation, autothermal reforming, oil pyrolysis, among others. However, the most common method is steam methane reforming (SMR). SMR is a catalytic process that breaks down hydrocarbons, primarily methane, into hydrogen and carbon monoxide, following the reactions below:

$$C_nH_m + nH_2O \rightleftharpoons nCO + (n + \frac{m}{2})H_2, \tag{2.1}$$

$$CH_4 + H_2O \rightleftharpoons CO + 3H_2 \quad \Delta H_R^0 = 206.3 \text{ kJ / mol}, \tag{2.2}$$

$$CO + H_2O \rightleftharpoons CO_2 + H_2 \quad \Delta H_R^0 = -41.2 \text{ kJ / mol}. \tag{2.3}$$

Source: HERMESMANN; MüLLER (2022).

This reaction is endothermic, meaning it requires heat to occur, typically provided by steam, resulting in pollution both through direct CO_2 emissions and through the consumption of energy, which is commonly derived from fossil fuels. Reaction 2.3, known as the water-gas shift reaction, is employed to enhance hydrogen yield by converting a portion of the carbon monoxide generated in the previous step into carbon dioxide and hydrogen.

The SMR process is currently the most widely utilized method for hydrogen production, responsible for approximately two-thirds of global hydrogen output as of 2023 (PAVAN et al., 2025). SMR plants can achieve capacities as high as 120,000 $Nm^3\ h^{-1}$ (HERMESMANN; MüLLER, 2022) and represent a mature, well-established technology with a technology readiness level (TRL) of 9 (HERMESMANN; MüLLER, 2022). There are other polluting hydrogen production methods, notably those utilizing coal, which account for 20% of global hydrogen production (PAVAN et al., 2025).

2.1.1.2 Blue Hydrogen

Blue hydrogen is produced in the same manner as grey hydrogen, with the sole difference being that part of the CO_2 produced in the process is captured and stored in geologic sites, hopefully, forever. This process is called carbon capture and storage (CCS).

"Capture efficiencies range from 53 to 95%, and can be increased albeit on expense of higher energy demands. It should be noted that the SMR plant efficiencies are reduced by 5-14% upon implementing CCS." (HERMESMANN; MüLLER, 2022).

2.1.1.3 Turquoise Hydrogen

Turquoise hydrogen is produced using methane pyrolysis (MP), a process that uses high temperatures to crack methane into hydrogen and solid carbon, as shown in the following reaction:

$$CH_4 \rightleftharpoons 2H_2 + C \quad \Delta H_R^0 = 74.9\ \text{kJ / mol.} \tag{2.4}$$

Source: HERMESMANN; MüLLER (2022).

"Common challenges that need to be overcome for scale-up of MP to commercial H_2 production are: (1) supplying the significant demand for heat to obtain reasonable space-time-yields, (2) handling the deposition of solid carbon on the surface of the catalyst and inside of

the reactor, (3) using natural gas instead of pure methane as a feedstock including the impact of the gas composition on process performance and product gas purity, and (4) further treating and commercially exploiting the solid carbon." (HERMESMANN; MüLLER, 2022).

2.1.1.4 Green Hydrogen

Hydrogen is referred to as green when it is produced through water electrolysis, as this method relies solely on water and electricity, which - when sourced from renewable energy - results in no significant pollutant emissions. The process is described by the following equation:

$$H_2O \rightleftarrows \frac{1}{2}O_2 + H_2 \quad \Delta H_R^0 = 285.9 \text{ kJ / mol.} \tag{2.5}$$

Source: HERMESMANN; MüLLER (2022).

To provide the necessary energy for water to undergo electrolysis, an electrolytic cell containing water and two electrodes connected to a direct current source is required. This setup creates a difference of electric potential, or voltage. A theoretical minimum voltage of 1.48 V has been calculated; however, due to practical system inefficiencies - such as losses at the electrodes, mass transport limitations, and ohmic resistance - the actual voltage required is higher. Consequently, the voltage efficiency is defined as the ratio between the theoretical and actual voltages (HERMESMANN; MüLLER, 2022).

Additionally, it is beneficial to differentiate between hydrogen production processes using steam and those using liquid water. When water is supplied as steam, the energy required for evaporation is already accounted for. Thus, considering the energy content of hydrogen based either on its higher heating value (HHV), used when water is provided in liquid form (3.54 kWh/Nm^3), or its lower heating value (LHV), used when water is supplied as steam (3.00 kWh/Nm^3), it becomes possible to calculate the overall efficiency of the hydrogen production system. This efficiency is determined by comparing these standard energy values with the actual electrical consumption (W_{el}) necessary to produce 1 Nm^3 of hydrogen under standard conditions, as follows:

$$\eta_{LHV} = \frac{\text{LHV}}{W_{el}}, \quad \eta_{HHV} = \frac{\text{HHV}}{W_{el}}. \tag{2.6}$$

Source: HERMESMANN; MüLLER (2022).

"The three most common electrolysis technologies to produce H_2 are alkaline water electrolysis (AEL), polymer electrolyte membrane water electrolysis (PEMEL) and

high-temperature, respectively solid oxide water electrolysis (SOEL). Electrolysis technologies mainly differ in (1) stage of development, (2) electrolyte and charge carrier, (3) typical operating conditions, and (4) suitability for dynamic operation forced by a discontinuous power supply from renewable power plants" (HERMESMANN; MüLLER, 2022).

Table 2.3 is used to further compare the three technologies.

Table 2.3: Comparison of hydrogen production methods

	AEL	**PEMEL**	**SOEL**
Advantages	• Non-noble catalysts • Long-term stability • Relatively low cost • Cost-effective	• Good partial load range • Possibility of 100% efficiency • Compact system design • High gas purity • Dynamic operation	• Low production cost • Efficiency up to 100% ($>$ 100% if hot steam is used) • High-pressure operation • Lower electricity consumption • Best HHV efficiency
Disadvantages	• Low partial load range • Low operational pressures • Corrosive liquid electrolyte	• High cost of components (use of precious metals) • No dependable cost information • Possibly low durability • Acidic corrosive environment • Worst HHV efficiency	• Higher water consumption • Bulky system design • No dependable cost information • High component cost • Acidic corrosive environment

Continued on next page

Table 2.3 – continued from previous page

	AEL	**PEMEL**	**SOEL**
Technology readiness level (TRL)	9	6-8	5

Sources: HELMEISTER (2024), CARMO et al. (2013), TELLO et al. (2025), PINSKY et al. (2020). Information arranged by the author.

2.2 Clean Energy

As explained in Section 2.1.1.4, it is of utmost importance to produce hydrogen using clean energy; otherwise, the objective of decarbonizing the economy cannot be achieved, irrespective of the use of electrolysis.

According to SVENSSON (2023), for hydrogen to qualify as a "renewable liquid and gaseous fuel of non-biological origin" under current EU legislation, the electricity employed in its production must originate from renewable energy sources **other than biomass**. Alternatively, electricity can be sourced from the public power grid, provided that the bidding zone in which the transaction occurs has either more than 90% renewable energy in its electricity mix or an emission intensity below 18 gCO_2e/MJ. Consequently, using this very formulation, the only viable approach for producing green hydrogen in Brazil involves a co-located "island" configuration, where the electrolyzer is directly connected to a renewable energy source, such as wind or solar, and operates independently from the public power grid. This necessity arises because Brazil has notably remained just below the 90% threshold of renewable energy share in its power mix between 2001 and 2020 (International Energy Agency (IEA), 2025), and its grid's emission intensity has fallen below the required limit in only four years from 2011 to 2023 (Ministério da Ciência, Tecnologia e Inovação, 2024).

2.2.1 Solar Energy

Solar photovoltaic (PV) power systems convert sunlight into electricity through the photovoltaic effect, which is the generation of voltage or electric current in a material when it is exposed to light. The power generated by the PV system at a given instant t can be described by the following equation:

$$P_{PV,t} = C_{PV}\,\eta_{PV} \cdot \left(\frac{G_{T,t}}{G_{T,STC}}\right) \cdot [1 + \alpha_P (T_{C,t} - T_{C,STC})], \tag{2.7}$$

where C_{PV} is the rated capacity of the PV array, η_{PV} represents the PV derating factor (efficiency), $G_{T,t}$ is the incident solar radiation at time t, and $G_{T,STC}$ is the incident solar radiation under Standard Test Conditions (STC). α_P denotes the PV cell temperature coefficient of power, while $T_{C,t}$ and $T_{C,STC}$ correspond to the PV cell temperature at time t and under STC, respectively.

Source: HASSAN et al. (2023).

Table 2.4 further analyzes the strengths and weaknesses of photovoltaic systems.

Table 2.4: Strengths and Weaknesses of Solar PV Systems

Strengths	**Weaknesses**
1. Renewable energy source: solar PV systems tap into abundant sunlight, providing a consistent and renewable source of energy for power generation.	**1. Intermittency:** solar energy production is limited to daylight hours and can be affected by weather conditions, leading to variability in output.
2. Predictable daily pattern: daily solar energy patterns are relatively predictable, allowing for better energy generation forecasts and grid integration.	**2. Nighttime generation:** solar panels do not produce energy at night, necessitating energy storage or alternative power sources during dark hours.
3. Scalability: solar arrays can be expanded by adding more panels, increasing energy production to match growing demand.	**3. Seasonal variations:** solar energy output can vary with the changing angle of the sun throughout the year, affecting overall annual production.
4. Low operating costs: solar PV systems have minimal operating costs after installation, as they do not require fuel or ongoing resource inputs.	**4. High initial costs:** the upfront cost of solar panel installation and equipment can be relatively high, impacting initial return on investment.
5. Decentralized generation: solar panels can be installed on rooftops and distributed across various locations, reducing strain on centralized power infrastructure.	**5. Shading impact:** shading on even a small part of a solar panel can significantly reduce energy production from the entire panel or string.

Continued on next page

Table 2.4 – continued from previous page

Strengths	Weaknesses
6. Environmental benefits: solar power reduces greenhouse gas emissions and air pollution, contributing to a cleaner environment and mitigating climate change.	**6. Limited energy generation in low light conditions:** energy production decreases significantly in cloudy, rainy, or heavily shaded conditions.
7. Low maintenance: solar panels require minimal maintenance, with no moving parts, reducing operational complexities and costs.	**7. Aesthetic considerations:** the appearance of solar panels might not always align with architectural preferences or community aesthetics.
8. Technological advancements: ongoing advancements improve solar panel efficiency, enhancing energy capture and reducing overall costs.	**8. Geographical limitations:** solar energy generation is location- dependent, with higher efficiency in regions with more sunlight.
9. Grid support: solar power can contribute to grid stability by generating power close to demand centers, reducing transmission losses.	**9. End-of-life management:** proper disposal and recycling of solar panels present challenges in minimizing environmental impact.
10. Energy independence: solar PV systems help diversify the energy mix and reduce dependence on fossil fuels, promoting energy security.	**10. Energy storage requirement:** storing excess solar energy for use during non-sunny periods requires efficient and cost-effective BT [Battery] technology.

Source: HASSAN et al. (2023).

2.2.2 Wind Power

"Wind power systems harness the kinetic energy of moving air to generate electricity, offering a sustainable and renewable source of energy. Wind turbines (WT), the primary components of these systems, consist of blades that capture wind energy and spin a rotor connected to a generator, producing electrical power through electromagnetic induction. The power output of a WT can be calculated as:

$$P_{WT,t} = 0.5 \cdot \rho \cdot A \cdot C_p \cdot v_t^3, \tag{2.8}$$

where $P_{WT,t}$ represents the power output, ρ is the air density, A is the swept area of the rotor, v_t is the wind speed, and C_p is the coefficient of performance that captures the efficiency of the

turbine energy conversion." (HASSAN et al., 2023).

The following table highlights the strengths and weaknesses of wind power systems:

Table 2.5: Strengths and Weaknesses of Wind Power

Strengths	**Weaknesses**
1. High energy yield: wind turbines can generate significant amounts of energy, especially in regions with consistent and strong wind resources.	**1. Intermittency:** wind energy production is variable due to fluctuations in wind speed, leading to inconsistent power output.
2. Predictable output: over the long term, wind patterns can be relatively predictable, enabling better energy production forecasts and grid integration.	**2. Low energy production in calm conditions:** wind turbines require a minimum wind speed (cut-in speed) to start generating power, leading to low energy production during calm conditions.
3. Scalability: wind farms can be expanded by adding more turbines, increasing energy production to meet growing demand.	**3. Shutdown in high wind:** turbines have a maximum wind speed (cut-out speed) at which they shut down to prevent damage, reducing energy production during strong winds.
4. Reduces fossil fuel dependence: wind power reduces the need for fossil fuel-based power generation, promoting energy security and reducing greenhouse gas emissions.	**4. Noise and aesthetic concerns:** noise generated by turbines and their visual impact can lead to community opposition, affecting the placement and operation of wind farms.
5. Low operating costs: once installed, wind turbines have relatively low operational costs compared to fuel- dependent power plants.	**5. Land use considerations:** wind farms require significant land area, which might compete with other land uses, such as agriculture or conservation.
6. Decentralized generation: wind farms can be distributed across different geographic locations, reducing strain on centralized power infrastructure.	**6. Resource limitations:** wind energy is location-specific, and not all areas have sufficient and consistent wind resources for reliable power generation.

Continued on next page

Table 2.5 – continued from previous page

Strengths	Weaknesses
7. Environmental benefits: wind power reduces air pollution, water usage, and greenhouse gas emissions, contributing to a cleaner environment.	**7. Maintenance challenges:** WT maintenance, especially for offshore installations, can be complex and require specialized equipment and personnel.
8. Grid stability: wind farms can provide grid support by helping to stabilize frequency and voltage fluctuations.	**8. Visual impact:** the visual presence of wind turbines in landscapes can lead to concerns about their impact on scenic views and tourism.

Source: HASSAN et al. (2023).

2.3 Ammonia

2.3.1 Ammonia Production

The most classic and widely used method for ammonia production is the Haber-Bosch process, which synthesizes ammonia by reacting nitrogen and hydrogen under high temperatures and pressures, as represented by the following reaction:

$$N_2 + 3H_2 \rightleftharpoons 2NH_3 \quad \Delta H_R^0 = -92.4 \text{ kJ / mol.} \tag{2.9}$$

Source: AZIZ; TRIWIJAYANTA; NANDIYANTO (2020).

In this work, the colours of ammonia are defined to be:

- Brown ammonia: produced with hydrogen and nitrogen originated from the reaction of methane with steam and air, coupled with the subsequent removal of water and CO_2 (AZIZ; TRIWIJAYANTA; NANDIYANTO, 2020).
- Blue ammonia: produced with blue hydrogen, regardless of the nitrogen source.
- Turquoise ammonia: produced with turquoise hydrogen, regardless of the nitrogen source.
- Green ammonia: produced with green hydrogen, regardless of the nitrogen source.

This nomenclature is consistent with SALMON; BAñARES-ALCáNTARA (2021).

To achieve the reaction conditions necessary for green ammonia production, one cannot simply heat the reactants using carbon-based fuels, as this would compromise the carbon-neutrality of the process. Instead, the required heat and mechanical work to reach the desired temperature and pressure must be supplied from renewable energy sources. One possible approach involves combusting a portion of the hydrogen produced, as explored in (SUN et al., 2024), which proposes a Rankine cycle based on hydrogen combustion with pure oxygen. However, since in this work it is assumed that the ammonia production plant is connected to a photovoltaic plant and the public grid, the energy required on those fronts will be supplied through electricity, either from the grid or from the photovoltaic plant.

2.3.2 Ammonia Storage and Transportation

Ammonia, being a toxic gas at room temperature and pressure, requires specific precautions for its storage and transportation. The most common approach involves liquefying the gas - either by compression or cooling - and storing it in pressurized tanks that can be transported by rail, road, or ship. It is also possible to transport ammonia via pipelines, eliminating the need for liquefaction.[2]

To store large volumes of liquid ammonia, it must either be pressurized to 8.58 bar at approximately 0 °C - a condition better suited for spherical or cylindrical tanks with a capacity of up to 1,500 tonnes - or cooled to -33 °C at atmospheric pressure, which is more appropriate for tanks of around 50,000 tonnes. In both cases, the choice of tank material is critical, since "ammonia is discordant with variant industrial materials and, in the presence of humidity, reacts with and corrodes different alloys of brass, zinc, and copper, forming a greenish/blue color" (KHAKSAR; RAHIMPOUR; RAHIMPOUR, 2024).

A summary of the storage tanks and their characteristics is presented in Table 2.6.

[2] According to KHAKSAR; RAHIMPOUR; RAHIMPOUR 2024, ammonia railcars can operate at pressures ranging from 0.2 to 3 MPa and at temperatures close to ambient.

Table 2.6: Ammonia Storage Tanks

Type	**Design temperature**	**Typical pressure (bar)**	**Refrigeration compressor**	**Capacity ammonia (metric tonnes)**
Refrigerated storage	-33°C	1.1 - 1.2	Two-stage	4500 - 45,000
Semirefrigerated storage	0°C - 5°C	3 - 5	One-stage	45 - 2700
Pressure storage	Ambient	16 - 18	None	< 270

Source: KHAKSAR; RAHIMPOUR; RAHIMPOUR (2024).

Figures 2.2 to 2.6 are taken from HIGNETT (1985) and offer valuable insights into the cost characteristics associated with this topic.

Figure 2.2: Estimated Capital Costs for Refrigerated Ammonia Storage Facilities

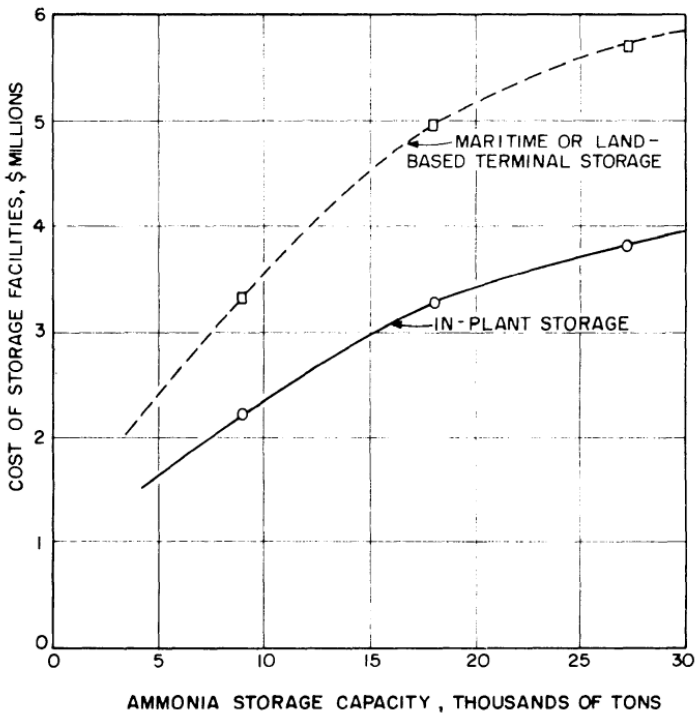

Figure 2.3: Pipeline Transportation Rates/ton-km

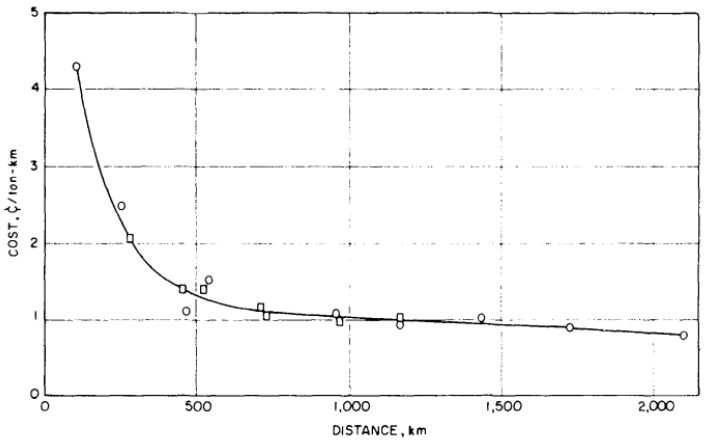

Figure 2.4: Terminal Charges for Various Space: Throughput Ratios

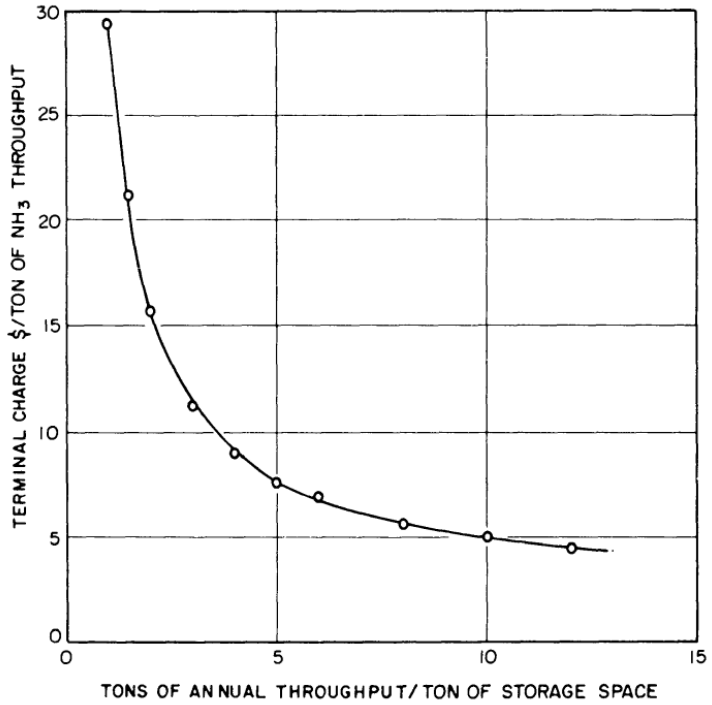

Figure 2.5: Truck Transportation Rates/ton-km as Related to Distance

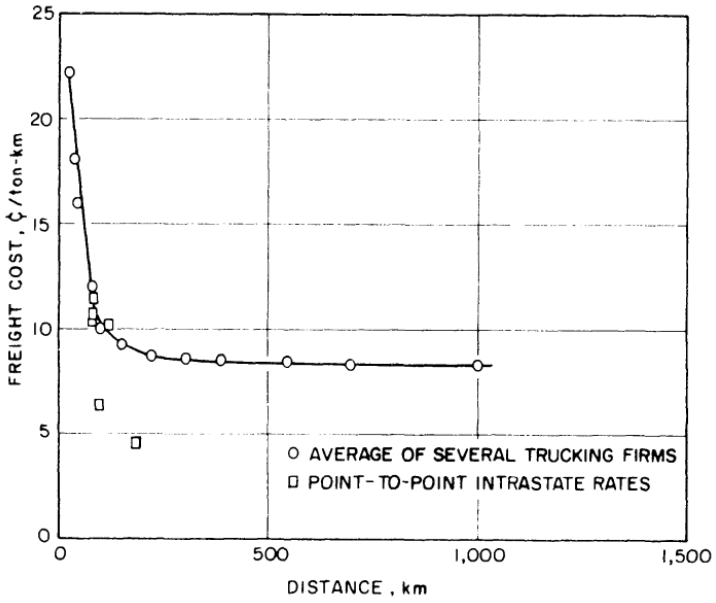

Figure 2.6: Comparison of Transportation Costs by Pipeline, Rail, and Truck

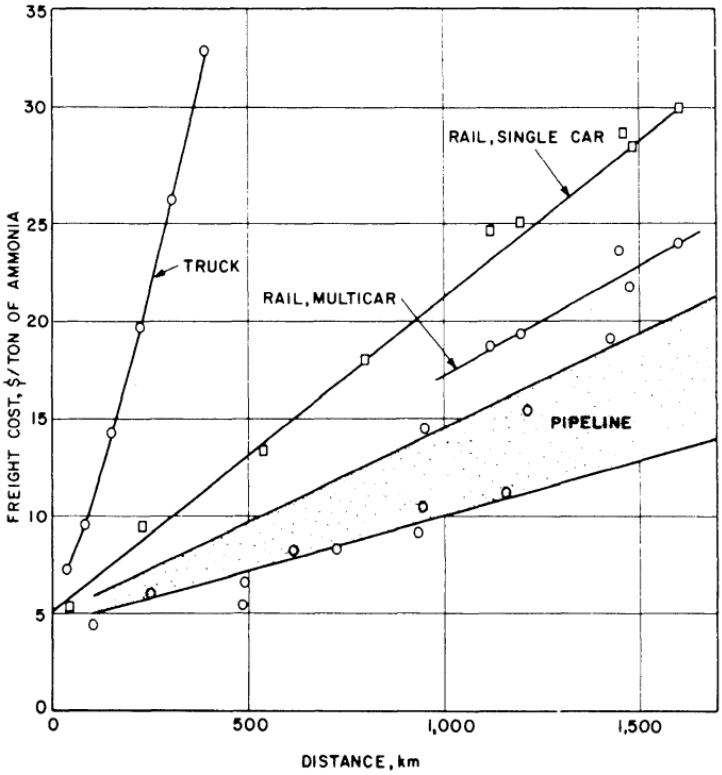

2.4 The Location Problem

2.4.1 Historical Background

A concise history of location theory can be drawn from standard monographs such as Daskin's *Network and Discrete Location* and the edited volumes by Drezner and Hamacher, as well as the more recent compendium in *Location Science* (DASKIN, 2013; DREZNER; HAMACHER, 2004; LAPORTE; NICKEL; GAMA, 2015). These sources narrate a progression from early *continuous* single-facility models toward *discrete* and *network-based* formulations that are now the backbone of supply-chain design. The early continuous models established the fundamental idea: locate a facility at a point in the plane to minimize a weighted measure of travel effort to multiple demand sites. Although deceptively simple, this viewpoint introduced the central trade-off between proximity to dispersed demand and economies achieved by concentrating capacity (DASKIN, 2013; DREZNER; HAMACHER, 2004).

Building on that foundation, the literature evolved to *discrete* models where facilities must be chosen from a finite set of candidate sites, typically embedded in a transportation network. Textbook treatments present the p-median model as the canonical formulation when the number of facilities is fixed (DASKIN, 2013). The p-median balances coverage and travel, selecting p sites so that each customer is assigned to its nearest open facility and total (or average) distance is minimized. Closely related is the uncapacitated facility-location framework, which makes the number of facilities be endogenous to the problem by trading off fixed opening costs against assignment (transport) costs. The uncapacitated model captures a core managerial tension: opening more facilities reduces distance but increases fixed cost; opening fewer facilities saves on fixed cost but lengthens average hauls. Modern expositions show both problems as compact mixed-integer linear programs and discuss exact and heuristic algorithms that scale to realistic instances (DASKIN, 2013; DREZNER; HAMACHER, 2004; LAPORTE; NICKEL; GAMA, 2015).

These textbooks also emphasize how the classical models have been extended: capacities and service-level constraints, multiple commodities and echelons, modular or discrete sizing of plants, as well as nonlinearities arising from economies of scale or physics. The result is a spectrum ranging from tractable MILPs for many design questions to genuinely MINLP formulations when nonlinear cost or engineering relations are essential. This evolutionary arc—from point-location ideas to discrete network design, and from linear cost structures to integrated (possibly nonlinear) supply-chain models—is thoroughly documented and provides the conceptual template for contemporary energy-infrastructure planning (LAPORTE; NICKEL; GAMA,

2015).

2.4.2 Modeling Approaches

2.4.2.1 Linear Programming (LP)

Linear programming occupies a useful, if specialized, niche in location analysis. Pure LP arises naturally when location choices are fixed in advance or when decisions can be modeled as continuous allocations without on/off (binary) commitments. Classic examples include network flow formulations in which production and shipment levels are continuous and costs are linear, or continuous single-facility models under rectilinear distances where the objective can be decomposed into independent one–dimensional median problems. In discrete location settings, however, the central managerial question—*should a facility be opened at a given site?*—is intrinsically binary. Consequently, LP is most valuable as a relaxation that provides lower bounds, as a building block inside decomposition frameworks, or as a vehicle for sensitivity analysis (LAPORTE; NICKEL; GAMA, 2015).

2.4.2.2 Mixed-Integer Linear Programming (MILP)

Mixed-integer linear programming is the canonical framework for discrete location problems. It expresses the core trade-offs of facility location with clarity: binary variables capture opening decisions, continuous variables capture assignments or flows, and a linear objective aggregates fixed and transport costs. The p-median model, for instance, fixes the number of facilities and minimizes total (or average) assignment distance, while the uncapacitated facility location model (UFLP) endogenizes the number of sites by balancing fixed opening costs against distribution costs. Capacitated variants add linear side-constraints, multi-commodity models couple several products through shared capacities, and multi-echelon formulations embed location decisions across tiers of a network. Decades of research—summarized in authoritative texts—have produced a mature algorithmic toolbox: tight formulations with strong valid inequalities, Benders and Lagrangian decompositions and highly effective branch-and-cut implementations in modern solvers (LAPORTE; NICKEL; GAMA, 2015). In practice, MILP strikes a pragmatic balance between modeling fidelity and tractability, enabling exact or provably near-optimal solutions for large, realistic instances.

2.4.2.3 Mixed-Integer Nonlinear Programming (MINLP)

When linear cost structures are insufficient—or when physics and economies of scale must be modeled explicitly—location design naturally becomes a mixed-integer *nonlinear* program. Typical sources of nonlinearity include concave cost-to-capacity curves (reflecting economies of scale), nonlinear transport or conversion relations (e.g., hydraulic or thermodynamic laws), and engineering performance envelopes that cannot be credibly linearized without material loss of fidelity. In energy and process systems, MINLP formulations frequently appear when siting production plants, storage, and conversion assets is integrated with design or operation variables—pipeline or compressor sizing, unit load–dependent efficiencies, or piecewise thermodynamic models. Contemporary reviews of hydrogen supply chains report both MILP and MINLP models: the former when cost curves and network physics are linearized or approximated; the latter when accurate flow/technology relations are essential to the investment decision (RIERA; LIMA; KNIO, 2023). The location problem thus becomes one layer in a tightly coupled design-and-planning model. Where possible, convexification and piecewise-linear approximations restore MILP tractability; otherwise, global or spatial-branch-and-bound MINLP solvers are employed, often assisted by problem-specific decompositions (LAPORTE; NICKEL; GAMA, 2015; RIERA; LIMA; KNIO, 2023).

2.4.3 Contemporary Relevance and Applications

Location problems remain central to the design of modern energy supply chains, particularly in the transition toward low-carbon vectors such as hydrogen and ammonia. Contemporary reviews emphasize that choosing where to site production plants, storage hubs, ports, pipelines, and refueling infrastructure is often the dominant driver of system cost and feasibility. In these studies, classical location–allocation logic is embedded within broader network design models that also account for technology choices, temporal operations, and policy constraints. A recent survey of hydrogen production and supply-chain optimization synthesizes a couple of decades of models and shows that facility siting (together with sizing and network layout) appears in nearly all formulations, from stylized planning exercises to detailed, country-scale case studies (RIERA; LIMA; KNIO, 2023). That literature also documents the spectrum of mathematical approaches in use today: MILP dominates when costs and physics can be linearized credibly, whereas MINLP (or MILP with rich piecewise approximations) is adopted when nonlinearities from economies of scale or engineering relations are material.

Applications specific to hydrogen illustrate these trends. National and regional studies formulate network-wide MILPs that co-optimize electrolyzer siting, storage placement, and

multimodal transport under carbon and cost targets; the location decisions determine whether distributed production with short hauls or clustered hubs with longer trunk movements are preferred. Recent case studies report that optimal layouts hinge on renewable resource geography, grid access, and demand density, and they increasingly explore uncertainty (prices, policy, technology costs) through stochastic or robust variants—again with location variables at the core of the design (RIERA; LIMA; KNIO, 2023). As models expand to energy-system scale, reviews note a growing need to reconcile fine spatial siting with temporal operations and cross-sector couplings, without losing tractability (LUECKEL; MONAGHAN; LYNCH, 2025).

Parallel developments are visible for ammonia, both as a decarbonized chemical and as a hydrogen carrier. Supply-chain studies now integrate siting of green ammonia plants with upstream renewable availability and downstream logistics to agriculture, industry, or export terminals. Methodologically, they adopt MILP superstructures—with capacity expansion and location decisions—to compare alternative routes (e.g., biomethane or ethanol-based pathways, electrolysis + Haber–Bosch), and they quantify how siting near resources versus near demand reshapes levelized costs and investment timing (GARCIA; PALACIOS; ENSINAS, 2024). Planning work on the transition of incumbent ammonia networks similarly embeds facility location within multi-year expansion models, using stochastic programming to treat demand and price uncertainty while preserving tractable solution times (MITRAI; PALYS; DAOUTIDIS, 2024). Across these efforts, the enduring insight is that *where* assets are placed—and at what modular sizes—largely fixes subsequent operating cost, emissions, and resilience, making location a first-order decision in the energy transition.

2.5 Levelized Cost of X

The levelized cost of a given output is a widely used metric to assess the average cost per unit of that a given output over the lifetime of its production facility. It is commonly applied to energy generation (Levelized Cost of Energy - LCOE), but can also be extended to other products, such as hydrogen (Levelized Cost of Hydrogen - LCOH) (NYANGON; DAREKAR, 2024) or ammonia (Levelized Cost of Ammonia - LCOA) (NAYAK-LUKE; BAñARES-ALCáNTARA, 2020).

The general formula for calculating the metric is given by:

$$\text{LCOX} = \frac{NPV(\text{of total cost over the lifetime of the plants})}{NPV(\text{of X produced over the power plant lifetime})}, \tag{2.10}$$

Source: Adapted from KABEYI; OLANREWAJU (2023),

where NPV stands for Net Present Value, and X represents the product being evaluated (energy, hydrogen, ammonia, etc.). The usage of NPV allows for the consideration of the time value of money, discounting future costs to their present values and also discounting the future production of X over time.

2.5.1 Historical Development

The "levelized" idea emerged in electricity planning as a lifecycle unit-cost that allocates upfront capital and ongoing operating expenditures over discounted lifetime output, offering a single comparative yardstick across technologies. Academic reviews refined definitions and highlighted sensitivity to key assumptions (discount rate, capacity factor, lifetime, fuel and carbon prices) and scope choices (taxes, transmission and distribution (T&D), integration costs) (SHORT; PACKEY; HOLT, 1995; IEA; NEA, 2020; BRANKER; PATHAK; PEARCE, 2011; FRIEDL et al., 2023).

From the late 2000s onward, critiques emphasized that plain LCOE is a *cost* metric and, by construction, ignores *value* differences caused by temporal and spatial profiles. For variable renewables, identical LCOEs can imply different system impacts and revenues depending on correlation with demand and with each other. This spurred "beyond-LCOE" proposals that either augment LCOE with explicit system integration components (e.g., System LCOE, LFSCOE) or pair costs with a value metric (e.g., VALCOE, LACE), aligning comparisons with market and adequacy realities (JOSKOW, 2011; UECKERDT et al., 2013; IEAGHG, 2020; TIMILSINA, 2020).

2.5.2 Recent Usage and Improvements

Today, LCOX is used well beyond power, because the same life-cycle accounting logic applies to any plant producing a measurable output over time (FRIEDL et al., 2023). Broad surveys and handbooks still present LCOE as a first-pass screening metric, but emphasize complementing it with system-aware measures (e.g., capacity credit, flexibility value, integration costs) (KABEYI; OLANREWAJU, 2023; TIMILSINA, 2020). In hydrogen, recent reviews synthesize LCOH ranges by pathway and policy context; in ammonia, techno-economic studies quantify LCOA under different renewable and plant-design assumptions (NYANGON; DAREKAR, 2024; NAYAK-LUKE; BAñARES-ALCáNTARA, 2020). Critical reviews also document frequent misuses (e.g., mixing financial and social discounting, inconsistent utilization assumptions), and recommend clarity about perspective (project vs. system) and boundaries (on-site vs. grid services) when reporting any LCOX figure (EMBLEMSVåG, 2025).

Furthermore, planning studies increasingly complement LCOE with "value-aware" metrics to avoid misleading rankings in systems with high variable renewable energy (VRE) shares. Four families stand out and motivate the sections below: VALCOE, which adjusts LCOE by energy, capacity, and flexibility value credits; LFSCOE, a full-system cost metric for meeting load reliably with a given technology plus least-cost complements; MLCOE, which adjusts levelization to a payback horizon or adds decision-relevant adjustments; and LACE, a revenue/benefit analogue to LCOE that measures avoided system costs per MWh. These appeared in response to policy needs for comparable yet system-aware indicators and have been applied in country-level portfolios and VRE integration studies (CEKIRGE; ERTURAN, 2019; LEAL; REGO; RIBEIRO, 2017; EMBLEMSVåG, 2025).

2.5.2.1 The Value-Adjusted Levelized Cost of Electricity (VALCOE)

VALCOE augments LCOE with a measured *value* component: energy value (hourly price times output), capacity value (resource's contribution to meeting peaks), and flexibility value (operational services), yielding a cost-versus-value comparison in a single indicator (International Energy Agency, 2020; IEAGHG, 2020; MANZOLINI et al., 2024). Conceptually, VALCOE asks whether a technology's discounted system value matches (or exceeds) its discounted cost, improving cross-technology comparisons when variable renewables and storage are prominent. Empirically, IEA applications show rank changes versus plain LCOE, particularly where capacity and flexibility have high marginal value (International Energy Agency, 2020).

About its calculation, VALCOE retains the standard cost denominator but subtracts per-MWh value credits for *energy*, *capacity*, and *flexibility* that a technology provides to the system:

$$\text{VALCOE} = \text{LCOE} - \left(v_{\text{energy}} + v_{\text{capacity}} + v_{\text{flex}}\right), \tag{2.11}$$

Source: Adapted from International Energy Agency (2024),

where each $v_{\cdot}$ is computed from market simulations or historical data as a discounted, output-normalized value component in \$/MWh. By embedding value, VALCOE improves cross-technology comparisons under diverse mixes and demand profiles (International Energy Agency, 2020; International Energy Agency, 2024).

2.5.2.2 The Levelized Full System Costs of Electricity (LFSCOE)

LFSCOE reframes evaluation at the market level: it defines the cost of serving the entire market with one technology plus storage (accounting for resource variability, storage losses,

and adequacy), then divides total discounted cost by total load served. This produces a "full-system" unit cost comparable across technologies and avoids LCOE's partial-equilibrium bias (IDEL, 2022). Case studies illustrate that LFSCOE for variable renewables can be an order of magnitude higher than project-level LCOE when the storage burden needed to achieve reliability is internalized, highlighting why project metrics and system metrics answer different questions (IDEL, 2022).

LFSCOE defines the unit cost of meeting load with a portfolio *built around* a target technology k and least-cost complements (storage, grid, dispatchables), ensuring adequacy and operating constraints:

$$\mathrm{LFSCOE}_k = \frac{\sum_{t=1}^{T} \frac{C_t^{\mathrm{sys}}(k)}{(1+i)^t}}{\sum_{t=1}^{T} \frac{E_t}{(1+i)^t}}. \tag{2.12}$$

Here C_t^{sys} aggregates investment and operating costs of all assets needed to reliably serve E_t and i is the discount rate. LFSCOE is closely related to "System LCOE" (UECKERDT et al., 2013) but frames a *meeting-load* experiment that is tractable for planning exercises; applications and formalization are provided in IDEL (2022), MATSUO (2022), BROWN; REICHENBERG (2021).

2.5.2.3 The Levelized Avoided Cost of Electricity (LACE)

LACE, developed by the United States Energy Information Administration (EIA), is the present value of revenues available to a candidate resource, i.e., the system's avoided cost of meeting the same energy and capacity needs with the existing/alternative mix—expressed per MWh. Comparing LACE to LCOE yields a value-to-cost ratio that screens economic attractiveness: projects with LACE>LCOE add net value in the modeled context (U.S. Energy Information Administration, 2013; U.S. Energy Information Administration, 2023). LACE addresses one core LCOE gap (market value), but still abstracts from many network and operational externalities; thus, it's best read alongside reliability and transmission assessments.

To calculate the metric, the following formula is used:

$$\mathrm{LACE} = \frac{\sum_{t=1}^{Y} \left(p_t^{\mathrm{marg}} \cdot h_t^{\mathrm{disp}}\right) \; + \; P^{\mathrm{cap}} \cdot \mathrm{CapCredit}}{H_{\mathrm{annual}}^{\mathrm{gen}}}, \tag{2.13}$$

where p_t^{marg} is the marginal generation price ($/MWh$) in period t; h_t^{disp} are dispatched hours; P^{cap} is the capacity payment ($/MW$·year); CapCredit is the capacity credit (fraction of name-

plate); $H_{\text{annual}}^{\text{gen}}$ is the annual expected generation hours.

Source: Adapted from U.S. Energy Information Administration (2013)

2.5.2.4 The Modified Levelized Cost of Electricity (MLCOE) and Modified Levelized Avoided Cost of Electricity (MLACE)

Several authors propose "modified" LCOE and LACE formulations to better reflect investor or policy perspectives. One strand, MLCOE/MLACE, replaces lifetime-average utilization with payback-period cash-flows and explicitly co-evaluates LCOE (cost) with LACE (value) for go/no-go screening; others incorporate integration adders or capacity credit into the numerator (CEKIRGE; ERTURAN, 2019). These modified metrics are pragmatic for project finance sensitivity analyses, but should be documented carefully (period, taxes, incentives, curtailment assumptions) to ensure reproducibility and comparability.

MLCOE variants adapt the levelization window and/or cost scope to investment decisions. A practical form replaces lifetime T by the payback horizon τ (or the economic life if shorter) and can include targeted adders (e.g., carbon pricing, grid fees):

$$\text{MLCOE} = \frac{\sum_{t=0}^{\tau} \frac{I_t + O_t + F_t}{(1+i)^t} + \sum_{t=\tau+1}^{T} \frac{A_t + O_t}{(1+i)^t}}{\sum_{t=1}^{T} \frac{E_t}{(1+i)^t}}, \tag{2.14}$$

$$\text{MLACE} = \frac{\sum_{t=0}^{\tau} \frac{R_t + C_t}{(1+i)^t} + \sum_{t=\tau+1}^{T} \frac{C_t}{(1+i)^t}}{\sum_{t=1}^{T} \frac{E_t}{(1+i)^t}}, \tag{2.15}$$

where

- I_t = levelized annual cost of plant financing,
- O_t = levelized annual operation and maintenance expenditure,
- F_t = levelized annual other expenditure (e.g., fixed costs),
- A_t = levelized annual adders (e.g., carbon pricing, grid fees),
- R_t = annual revenues (e.g., energy and capacity payments),
- C_t = annual system or capacity credits (avoided costs, policy incentives),

- E_t = amount of electricity produced annually,
- i = discount rate.

Source: Adapted from CEKIRGE; ERTURAN (2019).

3 METHODOLOGY

This chapter serves the purpose of detailing the methodology employed in this study, starting with the definition of the sets, variables, and parameters utilized in the mathematical model. Following this, a comprehensive explanation of the problem definition is provided, encompassing the various components involved in the production of green ammonia. Finally, the chapter concludes with a discussion on the location problem and the mathematical programming formulation used to address it, which is the central focus of this work.

3.1 Lists of Sets, Variables and Parameters

Table 3.1: List of Sets

Symbol	**Description**
L_c	Set of all the cities in the State of Mato Grosso
T	Set of all the years in the time horizon of the study

Table 3.2: List of Parameters

Symbol	**Units**	**Description**
$\eta_{\text{H-B}}$	-	Efficiency of the Haber-Bosch process
t_0	-	First year of operation
t_f	-	Last year of operation
Q_{MAI}	$\frac{\text{kWh}}{\text{kg of N}_2}$	Theoretical energy necessary to separate one kilogram of nitrogen from the air
$\eta^{\text{el}}_{\text{MAI}}$	-	Energy efficiency of the membrane air separation process

Continued on next page

Table 3.2 – continued from previous page

Symbol	Units	Description
$\theta^{\text{MAI}}_{\text{N}_2,\text{air}}$	$\frac{\text{kg of N}_2}{\text{kg of air}}$	Actual amount of nitrogen attained from one kilogram of pressurized air at the membrane air separation process
$\theta^{\text{MAI}}_{\text{O}_2,\text{air}}$	$\frac{\text{kg of O}_2}{\text{kg of air}}$	Actual amount of oxygen attained from one kilogram of pressurized air at the membrane air separation process
Q_{el}	$\frac{\text{kWh}}{\text{kg of H}_2}$	Theoretical energy necessary to produce one kilogram of hydrogen by the electrolysis process
$\eta^{\text{el}}_{\text{el}}$	-	Electrical efficiency of the electrolysis process
$\eta^{\text{m}}_{\text{el}}$	-	Massic efficiency of the electrolysis process
M_{H_2}	$\frac{\text{g}}{\text{mol}}$	Molar mass of hydrogen
M_{O_2}	$\frac{\text{g}}{\text{mol}}$	Molar mass of oxygen
M_{H_2O}	$\frac{\text{g}}{\text{mol}}$	Molar mass of water
M_{N_2}	$\frac{\text{g}}{\text{mol}}$	Molar mass of nitrogen
$\rho_{\text{PV},c}$	$\frac{\text{kW}}{\text{m}^2}$	Irradiance at city $c \in L_c$ (the mean value throughout one year)
η_{PV}	-	Efficiency of the photovoltaic panels
C_{PV}	$\frac{\text{US\$}_{t_0}}{\text{m}^2}$	Cost of photovoltaic panels
$\mathcal{N}$	-	Maximum number of plants that can be built at one location
$\dot{m}_{\text{NH}_3,\text{ min}}$	$\frac{\text{tonnes of NH}_3}{\text{day}}$	Minimum daily amount of ammonia production analyzed
$\dot{m}_{\text{NH}_3,\text{ max}}$	$\frac{\text{tonnes of NH}_3}{\text{day}}$	Maximum daily amount of ammonia production analyzed
$\text{C}^{\text{CAPEX}}_{\text{el, min}}$	$\text{US\$}_{t_0}$	Capital expenditure for the electrolyser process for minimal output plant
$\text{C}^{\text{CAPEX}}_{\text{H-B, min}}$	$\text{US\$}_{t_0}$	Capital expenditure for the Haber-Bosch process for minimal output plant
k	-	Literature parameter used to account for economies of scale
FC_{PV}	-	Value for the OPEX for the photovoltaic system expressed as a percentage of the CAPEX, per annum.
FC_{el}	-	Value for the OPEX for the electrolyser system expressed as a percentage of the CAPEX, per annum.

Continued on next page

Table 3.2 – continued from previous page

Symbol	Units	Description
$FC_{H\text{-}B}$	-	Value for the OPEX for the Haber-Bosch system expressed as a percentage of the CAPEX, per annum.
i	-	Discount rate
Δ_{c_1,c_2}	km	Geodesic distance between city $c_1 \in L_c$ and city $c_2 \in L_c$
δ	-	Circuity factor
C^{log}	$\frac{US\$_{t_0}}{tonne \cdot km}$	Cost of logistics per tonne of product per kilometer
P^{O_2}	$\frac{US\$_{t_0}}{tonne\ of\ O_2}$	Price of oxygen sold
$D_{c,t}^{NH_3}$	tonnes of NH_3	Demand for ammonia at location $c \in L_c$ at year $t \in T$
$D_{c,t}^{O_2}$	tonnes of O_2	Demand for oxygen at location $c \in L_c$ at year $t \in T$

Table 3.3: List of Variables

Symbol	Units	Description
$\dot{m}_2$	$\frac{kg\ of\ H\text{-}N\ mixture}{day}$	Daily amount of the hydrogen and nitrogen mixture heated and pressurized to be injected into the H-B reactor
$\dot{m}_3$	$\frac{kg\ of\ H\text{-}N\ mixture}{day}$	Daily amount of the hydrogen and nitrogen mixture to be heated and pressurized
$\dot{m}_4$	$\frac{kg\ of\ H_2}{day}$	Daily amount of hydrogen produced by the electrolysis process
$\dot{m}_5$	$\frac{kg\ of\ N_2}{day}$	Daily amount of nitrogen produced by the membrane air separation process
$\dot{m}_6$	$\frac{kg\ of\ water}{day}$	Daily amount of water pumped into the electrolysis process
$\dot{m}_7$	$\frac{kg\ of\ air}{day}$	Daily amount of pressurized air that goes into the membrane air separation process
$\dot{m}_8$	$\frac{kg\ of\ O_2}{day}$	Daily amount of oxygen produced by the electrolysis process
$\dot{m}_9$	$\frac{kg\ of\ O_2}{day}$	Daily amount of oxygen produced by the membrane air separation process
$\dot{m}_{10}$	$\frac{kg\ of\ O_2}{day}$	Daily amount of pressurized oxygen sold to local hospitals

Continued on next page

Table 3.3 – continued from previous page

Symbol	Units	Description
P_{PV}	kW	Power produced by the photovoltaic panels (the mean value throughout one year)
P_{el}	kW	Power used in the water electrolysis
S_{PV}	m^2	Area of the photovoltaic panels
$C^{\text{CAPEX}}_{PV,c}$	US$\$_{t_0}$	Capital expenditure for the photovoltaic panels at location $c \in L_c$
$C^{\text{CAPEX}}_{\text{el},c}$	US$\$_{t_0}$	Capital expenditure for the electrolyser at location $c \in L_c$
$C^{\text{CAPEX}}_{\text{H-B},c}$	US$\$_{t_0}$	Capital expenditure for the Haber-Bosch process at location $c \in L_c$
$\dot{m}_{\text{NH}_3,c}$	$\frac{\text{tonnes of NH}_3}{\text{day}}$	Daily ammonia production rate at location $c \in L_c$
$\lambda^{\text{NH}_3}_{c_1,c_2,t}$	Tonnes of NH_3	Amount of ammonia transported from location $c_1 \in L_c$ to location $c_2 \in L_c$ at year $t \in T$
$\lambda^{\text{O}_2}_{c_1,c_2,t}$	Tonnes of O_2	Amount of oxygen transported from location $c_1 \in L_c$ to location $c_2 \in L_c$ at year $t \in T$
y_c	-	Integer variable that indicates how many plants are built at location $c \in L_c$

3.2 Definition of the problem

The objective of this study is to analyze the costs associated with producing different amounts of green ammonia in Brazil, specifically in the state of Mato Grosso. This analysis will encompass the entire production process, from the generation of renewable energy to the final product. The general process of producing green ammonia is depicted in Figure 3.1, which illustrates the integration of renewable energy sources, such as solar and wind, with the production of green hydrogen and subsequently green ammonia, as explained in chapter 2.

Figure 3.1: General process of producing green ammonia.

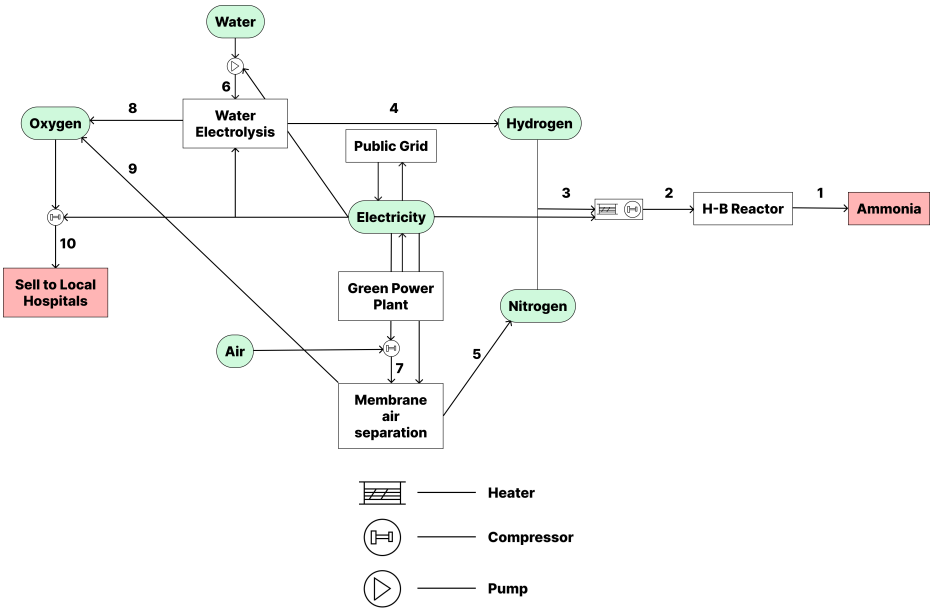

Source: Author

3.2.1 Balancing Equations

3.2.1.1 Green Power Plant

The "Green Power Plant" block represents the renewable energy generation system, which can be composed of either solar photovoltaic (PV) or wind energy sources. The choice of energy source is determined by the availability of resources in the region. A brief description of the characteristics of each energy source is provided in Section 2.2. In this study, the green power plant is modeled as a photovoltaic system, which is the most suitable option for the region of Mato Grosso.

Equation 3.1 represents the relationship between the power produced by the photovoltaic panels, the area of the panels, the irradiance at the location of the plant, and the efficiency of the panels.

$$S_{\mathrm{PV}} = \frac{P_{\mathrm{PV}}}{\rho_{\mathrm{PV},c} \cdot \eta_{\mathrm{PV}}}. \tag{3.1}$$

Since the power consumed by electrolysis is one to two orders of magnitude greater than the power consumed by the other processes (HUBERT et al., 2024; GARDINER, 2009; SIMOES et al., 2021), it is reasonable to approximate the power produced by the photovoltaic panels as being equal to the power consumed by the electrolysis process multiplied by a factor calculated

as the reciprocal of the portion of the total power consumption that is due to the electrolysis process, as calculated by SIMOES et al. (2021). This approximation is represented by Equation 3.2.

$$P_{\mathrm{PV}} \approx \frac{1}{88.4\%} \cdot P_{el}. \tag{3.2}$$

3.2.1.2 Water Electrolysis

The "Water Electrolysis" block represents the process of splitting water into hydrogen and oxygen using renewable energy, as discussed in Section 2.1.1.4. This work will consider the AEL technology for the electrolysis process, as it is the most ready for commercialization. The oxygen produced in this process is considered to be a byproduct and is sold to local hospitals. Equations 3.3 and 3.4 represent the mass balances for this process and, Equation 3.5 represents the power usage by the process. The factor $(24)^{-1}$ converts kWh / day to kW.

$$\dot{m}_6 = \frac{\dot{m}_4 + \dot{m}_8}{\eta_{\mathrm{el}}^{\mathrm{m}}}, \tag{3.3}$$

$$\dot{m}_8 = \frac{\mathrm{M}_{O_2}}{2\,\mathrm{M}_{H_2}} \cdot \dot{m}_4, \tag{3.4}$$

$$P_{el} = \eta_{\mathrm{el}}^{\mathrm{el}} \cdot Q_{\mathrm{el}} \cdot \dot{m}_4 \cdot (24)^{-1}. \tag{3.5}$$

3.2.1.3 Membrane Air Separation

The "Membrane Air Separation" block represents the process of separating nitrogen from the air. This process yields both nitrogen and oxygen: the nitrogen is the source of nitrogen for the ammonia synthesis, and the oxygen can be used in the same manner as the oxygen produced in the water electrolysis process. Equations 3.6 and 3.7 represent the mass balances for this process.

$$\dot{m}_5 = \theta_{\mathrm{N_2,air}}^{\mathrm{MAI}} \cdot \dot{m}_7, \tag{3.6}$$

$$\dot{m}_9 = \theta_{\mathrm{O_2,air}}^{\mathrm{MAI}} \cdot \dot{m}_7. \tag{3.7}$$

3.2.1.4 H-B Reactor

The "H-B Reactor" block represents the Haber-Bosch process, which is the chosen method for ammonia synthesis in this study. This process combines hydrogen and nitrogen to produce ammonia, as discussed in section 2.3.1. The heat and mechanical work required for this process are provided by the green electricity that is being discussed in this study. Equations 3.8 to 3.11 represent the mass balances for this process. The factor $\frac{1}{1000}$ is used to convert from kg/day to tonne/day.

$$\dot{m}_{\mathrm{NH_3}} = \frac{1}{1000} \cdot \eta_{\text{H-B}} \cdot \dot{m}_2, \tag{3.8}$$

$$\mathrm{M_{N_2}} \cdot \dot{m}_4 = 3\,\mathrm{M_{H_2}} \cdot \dot{m}_5, \tag{3.9}$$

$$\dot{m}_3 = \dot{m}_4 + \dot{m}_5, \tag{3.10}$$

$$\dot{m}_2 = \dot{m}_3. \tag{3.11}$$

3.2.1.5 Oxygen Compression

Oxygen gas is a valuable byproduct of the electrolysis and membrane air separation processes. However, in both cases, the oxygen produced is not in a state suitable for sale; therefore, it must be compressed using the energy produced by the green power plant. This energy is already accounted for by the assumption made in Equation 3.2. Equation 3.12 represents the mass balance for the oxygen compression process.

$$\dot{m}_{10} \leq \dot{m}_8 + \dot{m}_9. \tag{3.12}$$

3.2.2 Costs

Given what was discussed in the previous section, it is clear that the total cost of producing green ammonia is a function of the following variables:

- S_{PV}, since the cost of producing energy from solar panels is a function of the area of the panels.

- $\dot{m}_2$, since the cost of the heaters, compressors and the H-B reactor are a function of the amount of hydrogen and nitrogen that they need to process.
- $\dot{m}_6$, since the cost of the pumps and the cost of the water electrolysis equipment are a function of the amount of water that they need to pump.
- $\dot{m}_7$, since the cost of the air compressor and the cost of the membrane air separation equipment are a function of the amount of air that goes into the compressor.
- $\dot{m}_{10}$, since the cost of the oxygen compressor and the cost of the oxygen storage are a function of the amount of oxygen that they need to process and store.

The distribution of the production being the goal of this work, the costs can be reduced to a function of the amount of ammonia produced at each city, $\dot{m}_1$ and the irradiance $\rho_{\mathrm{PV},c}$, since all the other variables are dependent on these two. The logistics costs are also variable, as discussed in section 3.3.

3.3 The Location Problem

The location problem consists of determining the optimal locations and sizes of the green ammonia production plants, that is, deciding the optimum values for the decision variables $(\dot{m}_{\mathrm{NH_3},c}, \lambda^{\mathrm{NH_3}}_{c_1,c_2,t}, \lambda^{\mathrm{O_2}}_{c_1,c_2,t}, y_c)$. The problem is being modeled as a Mixed-Integer Nonlinear Programming (MINLP) problem, where the objective is to minimize the total costs (at present value)[1] of producing and distributing green ammonia that vary according to the aforementioned variables.

3.3.1 Objective Function

The objective function is a function of the decision variables and represents the costs that the model aims to minimize. It has four components, as shown below:

$$\min f(\dot{m}_{\mathrm{NH_3},c}, \lambda^{\mathrm{NH_3}}_{c_1,c_2,t}, \lambda^{\mathrm{O_2}}_{c_1,c_2,t}, y_c) = \mathrm{CAPEX} + \mathrm{OPEX} + \mathrm{LOGISTICS} - \mathrm{REVENUE}_{\mathrm{O_2}}, \quad (3.13)$$

where CAPEX is the capital expenditure of building the conversion plants, OPEX is the operational expenditure of producing ammonia, LOGISTICS is the cost of transporting ammonia

[1] This will also minimize the LCOA, since the model supposes perfect demand meeting at each year.

and oxygen from the conversion plants to the demand points, and REVENUE_{O_2} is the revenue generated from selling the byproduct oxygen.

The objective function is going to be used to obtain the LCOA (Levelized Cost of Ammonia) for the different plants, locations and for the whole system.

Equation 3.14 shows how the LCOA is calculated from the objective function for the whole system:

$$\text{LCOA} = \frac{f(\dot{m}_{\text{NH}_3,c}, \lambda^{\text{NH}_3}_{c_1,c_2,t}, \lambda^{\text{O}_2}_{c_1,c_2,t}, y_c)}{\sum_{t\in T}\sum_{c_1\in L_c}\sum_{c_2\in L_c}\lambda^{\text{NH}_3}_{c_1,c_2,t}\cdot(1+i)^{-(t-t_0)}}. \tag{3.14}$$

It is important to notice that the denominator of Equation 3.14 does not actually depend on the decision variables, since the total amount of ammonia produced in a certain year will always be equal to the total demand of that year, given the constraints of the model (see Section 3.3.2.1). Therefore, minimizing the objective function $f(\dot{m}_{\text{NH}_3,c}, \lambda^{\text{NH}_3}_{c_1,c_2,t}, \lambda^{\text{O}_2}_{c_1,c_2,t}, y_c)$ is equivalent to minimizing the LCOA.

3.3.1.1 CAPEX

The capital expenditure has a component that varies only with the size of the plant and one that also varies with the location of the plant. The cost related to solar panels is thought to vary linearly with the area of the panels, which is a function of the power consumed by the electrolysis process and the irradiance at the location of the plant, as shown in equation 3.1. The other components of the CAPEX are thought to vary exponentially with the amount of ammonia produced.

The cost associated with building the panels can be derived from equations 3.1, 3.2, 3.5 3.8, 3.9, 3.10 and 3.11, resulting in:

$$\text{C}^{\text{CAPEX}}_{PV,c} = \text{C}_{\text{PV}}\cdot\frac{1}{\rho_{\text{PV},c}\cdot\eta_{\text{PV}}}\cdot\frac{1}{88.4\%}\cdot\eta^{\text{el}}_{\text{el}}\cdot Q_{\text{el}}\cdot(24)^{-1}\cdot\frac{1000}{\eta_{\text{H-B}}\cdot\left(1+\frac{\text{M}_{\text{N}_2}}{3\text{M}_{\text{H}_2}}\right)}\cdot\dot{m}_{\text{NH}_3,c}. \tag{3.15}$$

It is worth noting that this cost has an inverse relationship with the irradiance at the location of the plant and a direct relationship with the maximum capacity installed at each location. This means that this particular cost is not much affected by economies of scale or the location of the plants (given that the irradiances of proximate cities don't vary harshly), and therefore, since this is expected to be the most significant component of the CAPEX, it is reasonable to assume

that this particularity will benefit the distributed production approach.

The cost associated with building the other components of the plant is split as follows:

$$\mathrm{C}_{\mathrm{el},c}^{\mathrm{CAPEX}} = \mathrm{C}_{\mathrm{el,\ min}}^{\mathrm{CAPEX}} \cdot \left[(y_c - 1) \cdot \left(\frac{\dot{m}_{\mathrm{NH_3,max}}}{\dot{m}_{\mathrm{NH_3,min}}} \right)^k + \left(\frac{\dot{m}_{\mathrm{NH_3},c} - (y_c - 1) \cdot \dot{m}_{\mathrm{NH_3,max}}}{\dot{m}_{\mathrm{NH_3,min}}} \right)^k \right]. \quad (3.16)$$

$$\mathrm{C}_{\mathrm{H\text{-}B},c}^{\mathrm{CAPEX}} = \mathrm{C}_{\mathrm{H\text{-}B,\ min}}^{\mathrm{CAPEX}} \cdot \left[(y_c - 1) \cdot \left(\frac{\dot{m}_{\mathrm{NH_3,max}}}{\dot{m}_{\mathrm{NH_3,min}}} \right)^k + \left(\frac{\dot{m}_{\mathrm{NH_3},c} - (y_c - 1) \cdot \dot{m}_{\mathrm{NH_3,max}}}{\dot{m}_{\mathrm{NH_3,min}}} \right)^k \right]. \quad (3.17)$$

This formulation allows for the modeling of multiple plants at the same location, but enforces that, at each city, an additional plant can only be built if the previous one has the maximum capacity possible. This is done both to simplify the model and computations and to have a more rationalized approach to building plants. One interesting property of this formulation is that it holds both when y_c is binary ($y_c \in \{0,1\}$) and when it can take integer values ($y_c \in \{0,1,2,\ldots,\mathscr{N}\}$).

The term representing the costs of the maximum capacity plants, $(y_c - 1) \cdot \left(\frac{\dot{m}_{\mathrm{NH_3,max}}}{\dot{m}_{\mathrm{NH_3,min}}} \right)^k$, is only in effect when $y_c > 1$ and depends only on the number of plants built with the maximum size (i.e., $y_c - 1$), and the other term accounts for the "last" plant that is not necessarily at maximum capacity. It becomes clear that for the "Small Plants" regime (see Section 3.4.1.4), this formulation allows for the same maximum capacity per city, but not per plant, which will make those costs be considerably higher, since the economies of scale will not be as effective.

The total CAPEX is given by:

$$\mathrm{CAPEX} = \sum_{c \in L_c} \left(\mathrm{C}_{PV,c}^{\mathrm{CAPEX}} + \mathrm{C}_{\mathrm{el},c}^{\mathrm{CAPEX}} + \mathrm{C}_{\mathrm{H\text{-}B},c}^{\mathrm{CAPEX}} \right). \quad (3.18)$$

3.3.1.2 OPEX

For simplification purposes, the variable cost is thought to be negligible when compared to the fixed cost. Let the present-worth factor over $t_f - t_0$ years be

$$a_{\overline{(t_f - t_0)}|i} = \frac{1 - (1+i)^{-(t_f - t_0)}}{i}. \quad (3.19)$$

Then the present value (in US$\$_{t_0}$) of OPEX is:

$$\text{OPEX} = a_{\overline{(t_f - t_0)}|i} \sum_{c \in L_c} \left(\text{FC}_{\text{PV}} \cdot \text{C}^{\text{CAPEX}}_{PV,c} + \text{FC}_{\text{el}} \cdot \text{C}^{\text{CAPEX}}_{\text{el},c} + \text{FC}_{\text{H-B}} \cdot \text{C}^{\text{CAPEX}}_{\text{H-B},c} \right). \tag{3.20}$$

This states that the OPEX is calculated as a percentage of the CAPEX, per annum, summed over the lifetime of the project and discounted to present value.

3.3.1.3 Logistics

The logistics costs are calculated as the sum of the costs of transporting one tonne of ammonia from each conversion plant to each demand point in each year, multiplied by the amount transported, as follows:

$$\text{LOGISTICS} = \sum_{t \in T} (1+i)^{-(t-t_0)} \sum_{c_1 \in L_c} \sum_{c_2 \in L_c} \left(\text{C}^{\log} \cdot \Delta_{c_1,c_2} \cdot \delta \cdot \left(\lambda^{\text{NH}_3}_{c_1,c_2,t} + \lambda^{\text{O}_2}_{c_1,c_2,t} \right) \right). \tag{3.21}$$

The cost of logistics is modeled to be directly proportional to the distance traveled and the amount transported, and the distance is calculated as the geodesic distance between the two cities multiplied by a circuity factor, to account for the fact that roads are not perfectly straight lines between each city.

3.3.1.4 Revenue from selling oxygen

The revenue generated from selling the byproduct oxygen is calculated as the sum of the revenues of selling one tonne of oxygen from each conversion plant to each demand point in each year, multiplied by the amount transported, as follows:

$$\text{REVENUE}_{O_2} = \sum_{t \in T} (1+i)^{-(t-t_0)} \sum_{c_1 \in L_c} \sum_{c_2 \in L_c} \left(\text{P}^{\text{O}_2} \cdot \lambda^{\text{O}_2}_{c_1,c_2,t} \right). \tag{3.22}$$

3.3.2 Constraints

The model has five sets of constraints, which are equalities and inequalities used to ensure that the system operates within its physical and logical limits.

3.3.2.1 Demand

This set of constraints ensures that the demand for ammonia at each demand point in each year is met by the sum of the amounts transported from all conversion plants. This ensures that there will not be any waste, accumulation, speculation, or shortage of ammonia, as follows:

$$\sum_{c_1 \in L_c} \lambda^{\mathrm{NH_3}}_{c_1,c_2,t} = \mathrm{D}^{\mathrm{NH_3}}_{c_2,t}, \quad \forall c_2 \in L_c, \forall t \in T. \tag{3.23}$$

The rationale behind this constraint is that the term $\sum_{c_1 \in L_c} \lambda^{\mathrm{NH_3}}_{c_1,c_2,t}$ amounts to the total ammonia received at location c_2 (from all conversion plants) in year t, and this must be equal to the demand of that year.

3.3.2.2 Conversion Plant Capacity

This set of constraints ensures that if a conversion plant is built at a certain location, its size must be between the minimum and maximum sizes allowed, and that the integer (or binary) variable related to the decision of how many plants to build at that location is set to the correct value, as follows:

$$\dot{m}_{\mathrm{NH_3},c} \leq \dot{m}_{\mathrm{NH_3,max}} \cdot y_c, \qquad \forall c \in L_c, \tag{3.24}$$

$$\dot{m}_{\mathrm{NH_3},c} \geq \dot{m}_{\mathrm{NH_3,max}} \cdot (y_c - 1) + \dot{m}_{\mathrm{NH_3,min}}, \quad \forall c \in L_c, \tag{3.25}$$

$$\dot{m}_{\mathrm{NH_3},c} \geq 0, \qquad \forall c \in L_c. \tag{3.26}$$

This ensures that if more than one plant is built at a certain location, the previous plants must be at maximum capacity, and that every plant built must be at least at minimum capacity. This property is assumed by the model, as specified in Section 3.3.1.1.

3.3.2.3 Conversion Plant Size

This set of constraints ensures that the amount of ammonia produced at a certain conversion plant in a certain year does not exceed the capacity of that plant, as follows:

$$\sum_{c_2 \in L_c} \lambda^{\mathrm{NH_3}}_{c_1,c_2,t} \leq 365.25 \cdot \dot{m}_{\mathrm{NH_3},c_1} \quad \forall c_1 \in L_c, \forall t \in T. \tag{3.27}$$

The rationale behind this constraint is that the term $\sum_{c_2 \in L_c} \lambda^{\mathrm{NH_3}}_{c_1,c_2,t}$ amounts to the total ammonia produced at location c_1 (and sent to any demand points) in year t, and this must be less than or equal to the maximum production capacity of that location, which is given by the daily production rate multiplied by the number of days in a year (365.25).

3.3.2.4 Oxygen Balance

This set of constraints ensures that the amount of oxygen transported from a certain conversion plant to a certain demand point in a certain year does not exceed the amount of oxygen that can be produced at that conversion plant (derived from inequality 3.12 and Equations 3.4, 3.6, 3.7, 3.8, 3.9, 3.10 and 3.11), nor the demand for oxygen at that demand point, as follows:

$$\sum_{c_2 \in L_c} \lambda^{\mathrm{O_2}}_{c_1,c_2,t} \leq \left(\frac{\mathrm{M_{O_2}}}{2\,\mathrm{M_{H_2}}} + \frac{\theta^{\mathrm{MAI}}_{\mathrm{O_2,air}}}{\theta^{\mathrm{MAI}}_{\mathrm{N_2,air}}} \cdot \frac{\mathrm{M_{N_2}}}{3\,\mathrm{M_{H_2}}} \right) \frac{1}{\eta_{\text{H-B}} \cdot \left(1 + \frac{\mathrm{M_{N_2}}}{3\,\mathrm{M_{H_2}}}\right)} \cdot \sum_{c_2 \in L_c} \lambda^{\mathrm{NH_3}}_{c_1,c_2,t} \qquad \forall c_1 \in L_c, \forall t \in T, \tag{3.28}$$

$$\sum_{c_1 \in L_c} \lambda^{\mathrm{O_2}}_{c_1,c_2,t} \leq \mathrm{D}^{\mathrm{O_2}}_{c_2,t} \qquad \forall c_2 \in L_c, \forall t \in T. \tag{3.29}$$

The rationale behind these constraints is that the term $\sum_{c_2 \in L_c} \lambda^{\mathrm{O_2}}_{c_1,c_2,t}$ amounts to the total oxygen produced at location c_1 (and sent to any demand points) in year t, and the term $\sum_{c_2 \in L_c} \lambda^{\mathrm{NH_3}}_{c_1,c_2,t}$ amounts to the total ammonia produced at location c_1 (and sent to any demand points) in year t. It follows that there is a maximum amount of oxygen that can be produced at each conversion plant, given by the product of the amount of ammonia produced that year at that plant and a conversion factor derived from the mass balances of the processes. Also, the term $\sum_{c_1 \in L_c} \lambda^{\mathrm{O_2}}_{c_1,c_2,t}$ amounts to the total oxygen received at location c_2 (from all conversion plants) in year t, and this must be less than or equal to the demand of that year. Usually, for bigger plants, the second set of constraints will be the limiting factor, and for small plants, the first set can be the bottleneck.

3.3.2.5 Domains

This set of constraints ensures that the model will not produce negative amounts of ammonia and that the integer (or binary) variables are constrained to take integer (or binary) values, as follows:

$$\lambda^{NH_3}_{c_1,c_2,t} \geq 0 \qquad \forall c_1 \in L_c, \forall c_2 \in L_c, \forall t \in T, \tag{3.30}$$

$$y_c \in \mathbb{Z},\ 0 \leq y_c \leq \mathscr{N} \qquad \forall c \in L_c. \tag{3.31}$$

Setting the domains of the other variables is not necessary, as they are constrained by the model elsewhere.

3.4 Solution Methodology

3.4.1 Data Collection

The data were collected through literature research and publicly available databases. However, a large part of the data used was not easily found in a single source, so it was necessary to combine data from multiple sources and make assumptions to fill in the gaps. Below, the rationale behind the estimation of the most important parameters used in this work is described; all the other parameters are described in Annex A.

3.4.1.1 Demand for Ammonia

The model requires a value for the demand for ammonia for each city in Mato Grosso for each year in the time horizon of the study. Historical data for the consumption of ammonia in Mato Grosso were calculated by a research group from the Chemical Engineering Department at the University of São Paulo that has agreed to provide the data for this work before publishing it (2025). The group used the data from IBGE about the agricultural production in each city of Brazil (IBGE, 2025) from 1974 to 2023 and data from the literature about the usage of ammonia-based fertilizers for each crop to estimate the total consumption of ammonia in each city of Mato Grosso in the same time period. They found multiple sources of information that had different estimates for the same parameter, so they recorded the minimum, maximum and average values for ammonia usage per crop, which generated three scenarios that will be used in this study and will be referenced as “min”, “avg” and “max” scenarios.

For the initial demand forecasting of ammonia, a Holt–Winters exponential smoothing (per city) method was implemented in Python, using the statsmodels library (SKIPPER; JOSEF, 2010), but the results were not realistic, as they predicted a linear growth that was almost 2.5 times the 2023 value. In reality, there will be a point in the future where the land usage will stabilize, either because of environmental regulations or because of the saturation of the market.

Therefore, the assumption was made that the growth of ammonia consumption in Mato Grosso would diminish over time until reaching a maximum value around 2030 (STABILE et al., 2020; Instituto Produzir, Conservar e Incluir (PCI), 2022). A sigmoid function was used to model this behavior, with the maximum value being 1.50×10^9 kg[2] of ammonia per year, reaching 99% in 2032, as shown in Figure 3.2.

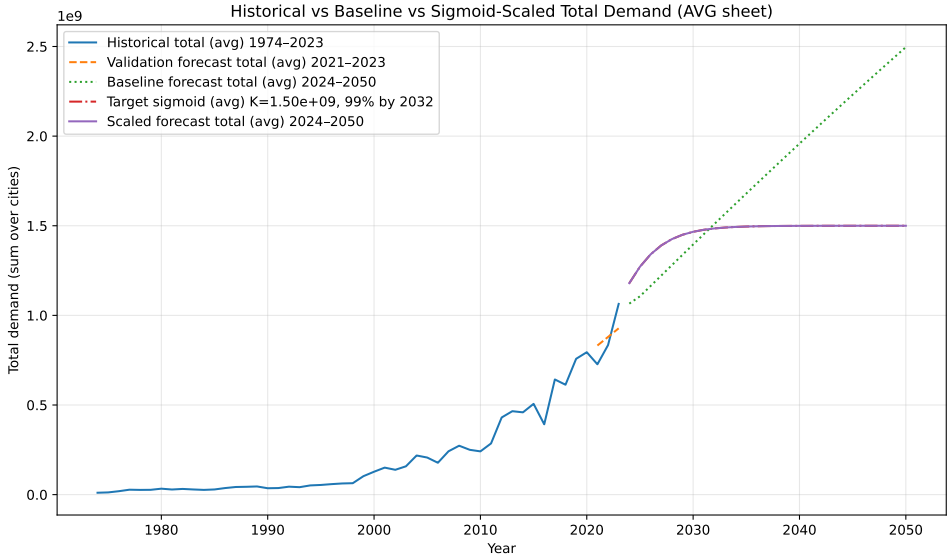

Figure 3.2: Forecast of the total ammonia demand in Mato Grosso from 1974 to 2050, using Holt–Winters exponential smoothing.

Source: Author, based on data from (DUTENKEFER et al., 2025)

Figure 3.2 shows the sum of the demand for ammonia in all cities of Mato Grosso from 1974 to 2023 (in blue), a validation of the forecast method for the last three historical data points (in dashed orange), the Holt–Winters baseline forecast (in dotted green), the target sigmoid (in red, however invisible due to it being perfectly behind the final forecast line), and the scaled forecast (in purple).

Heatmaps showing the estimated demand for ammonia at each city in Mato Grosso in 2026 and 2050 for the three scenarios (“min”, “avg” and “max”) are shown below.

[2]For the “min” scenario, the value was 8.87×10^8 kg and for the “max” scenario, the value was 2.18×10^9 kg

Figure 3.3: Ammonia demand in each municipality of Mato Grosso, Brazil, in 2026, for different scenarios.

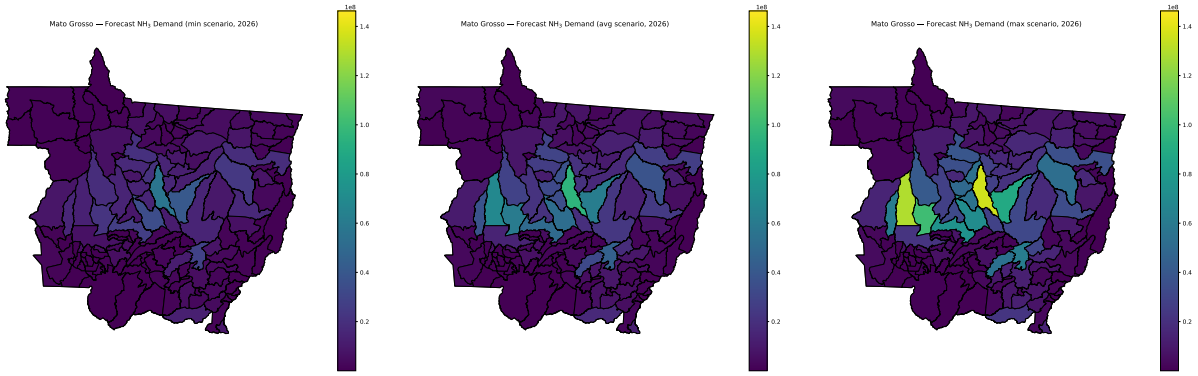

(a) “Min” scenario (b) “Avg” scenario (c) “Max” scenario

Source: Author, based on data from DUTENKEFER et al. (2025)

Figure 3.4: Ammonia demand in each municipality of Mato Grosso, Brazil, in 2050, for different scenarios.

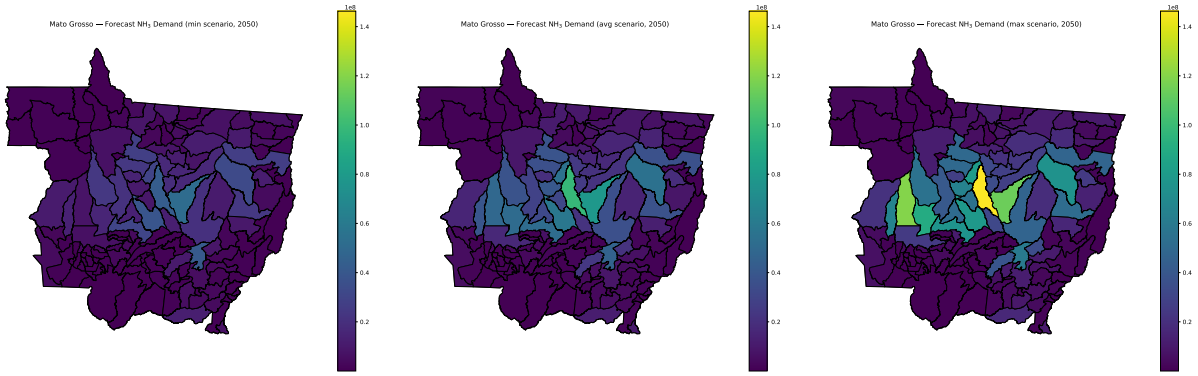

(a) “Min” scenario (b) “Avg” scenario (c) “Max” scenario

Source: Author, based on data from DUTENKEFER et al. (2025)

One can observe that, by the way the data were obtained, the demand for ammonia is more prevalent in the middle (latitude-wise) of the state, and this tendency is more pronounced in the later years and in the “max” scenario. Although a more detailed forecast could be proposed, this is sufficient to generate interesting test cases to observe the behavior of a decentralized production system for green ammonia.

3.4.1.2 Demand for Oxygen

The model requires a value for the demand for oxygen in each city in Mato Grosso for each year in the time horizon of the study. GóMEZ-CHAPARRO; GARCíA-SANZ-CALCEDO; MáRQUEZ (2018) reported that the amount of oxygen used yearly per hospital bed is estimated to be 350 m^3, which is equivalent to 0.50015 tonnes of O_2 per bed per year (MCCAMY,

1956). Therefore, the yearly demand for oxygen for each city can be estimated by multiplying the number of hospital beds in that city by this factor. The number of hospital beds in each city of Mato Grosso was obtained from the Brazilian Ministry of Health database (2025). For simplicity, it was assumed that the demand for oxygen would not vary over the years.

The figure below shows a heatmap of the estimated demand for oxygen in each city in Mato Grosso.

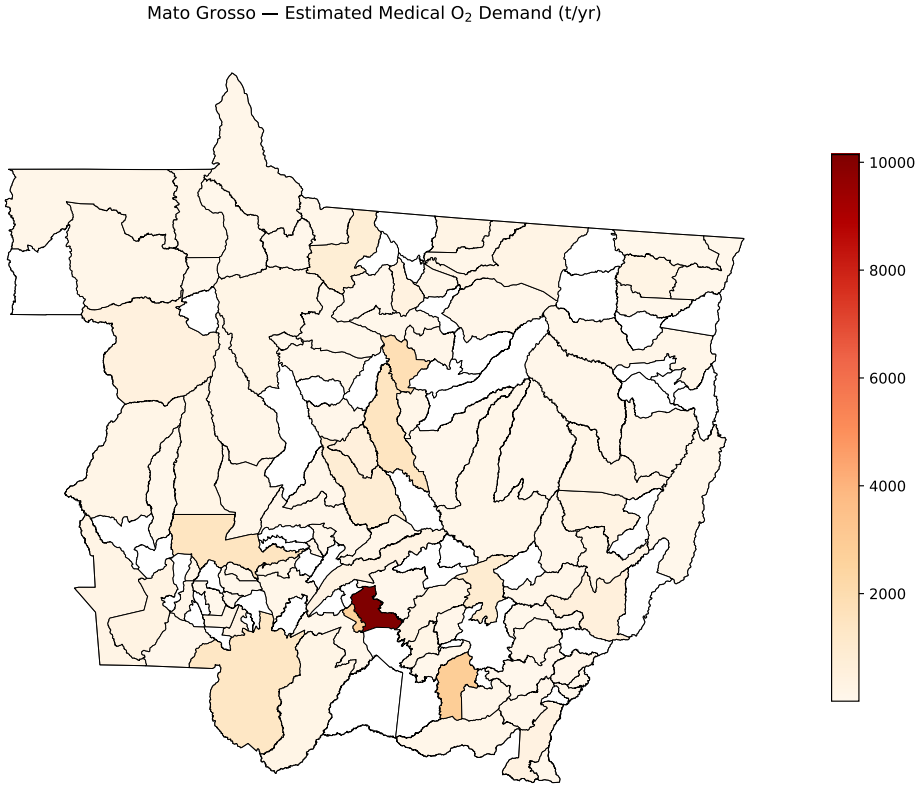

Figure 3.5: Oxygen demand in each municipality of Mato Grosso, Brazil.
Source: Author, based on data from (GóMEZ-CHAPARRO; GARCíA-SANZ-CALCEDO; MáRQUEZ, 2018; MCCAMY, 1956; Brasil. Ministério da Saúde. Departamento de Atenção Hospitalar, Domiciliar e de Urgência (DAHU). Coordenação-Geral de Atenção Hospitalar e Domiciliar (CGHID), 2025)

It is interesting to note that the state capital Cuiabá has around four times the demand for oxygen of the second most demanding city, Rondonópolis, and around 25 times the demand of the average non-zero-demand city. This might favor the construction of a large conversion plant near Cuiabá, as it would be able to avoid long-distance transportation of oxygen to that city.

3.4.1.3 Discount Rate

A value for the discount rate must be chosen to calculate the present value of future costs and yields. The discussion about the appropriate value for the discount rate is extensive and outside the scope of this work; therefore, a nominal value of 15% per year was chosen, which is a reasonable value for projects in Brazil, given the current economic situation of the country.

3.4.1.4 Plant Sizing

To ensure a distributed production system, two regimes were considered for the maximum production at each municipality, which are:

- "Small Plant" Regime: maximum production of 100 tonnes of ammonia per day and a maximum of five plants per municipality.
- "Medium Plant" Regime: maximum production of 500 tonnes of ammonia per day and a maximum of one plant per municipality.

It is logically necessary that the "Medium Plant" regime has a lower total cost of production per tonne of ammonia, given that larger plants have economies of scale, however, the "Small Plant" regime is more realistic, since it enables the plants to be distant of each other, potentially improving the usage of infertile lands for energy generation and reducing the logistics costs, given that the plants can be built closer to the demand points.

Besides being more realistic, the "Small Plant" regime also serves a social purpose, as it distributes the labour opportunities among more municipalities, potentially improving the local economies of smaller cities. One of the biggest factors that make the economies of scale to be such an effective force for chemical plants is due to the amount of employees needed to run the plant, which does not scale linearly with the size of the plant, in fact, larger plants tend to have a much lower number of employees of every area (engineers, operators, salesmen, accountants, etc.) per tonne of product produced.

3.4.2 Model Implementation

The model was implemented using the Python programming language and the Gurobi optimization solver (Gurobi Optimization, LLC, 2025). The solver has two built-in methods for dealing with non-linearity, which are the static piecewise linear approximation and the spatial branch-and-bound method. The static piecewise linear approximation method was tested and

quickly discarded, as it was considerably slower than the other method, which was used for all the results presented in this work.

Gurobi's version 12.0.3 build v12.0.3rc0 (linux64 - "Arch Linux") was used for all the simulations, running on a computer with CPU model: Intel(R) Core(TM) i5-10300H CPU @ 2.50GHz, instruction set [SSE2—AVX—AVX2]. Thread count: 4 physical cores, 8 logical processors, using up to 8 threads. The run logs state that the model has 994473 continuous and 141 integer (or binary) variables, but its presolve phase reduces it to 821749 continuous and 141 integer (or binary) variables. One can observe that, by having 141 continuous variables for $\dot{m}_{\mathrm{NH}_3,c}$, $141 \times 141 \times 25$ continuous variables for both $\lambda^{\mathrm{NH}_3}_{c_1,c_2,t}$ and $\lambda^{\mathrm{O}_2}_{c_1,c_2,t}$, and 141 integer (or binary) variables for y_c, the model is still short of 2×141 continuous variables; those are auxiliary variables needed to model the non-linear parts of the model using the spatial branch-and-bound method.

The tolerated maximum optimality gap was set to 1% for all of the runs, which means that the solver would stop when it found a solution that was within 1% of the optimal solution. This proved to be a good compromise between solution quality and computation time, as the runs were taking up to eight hours to complete, especially for the "Medium Plant" regime. The fact that the regime using binary variables took more time to solve than the one using integer variables is counter-intuitive, but it is likely due to the fact that the binary regime has a larger feasible region to explore, given that the effective maximum capacity per plant is higher. In addition, the economies of scale (which is precisely the non-linear part of the model) are more pronounced in the "Medium Plant" regime, which likely makes the solver take more time to explore the non-linearities of the model.

With regard to the sensitivity analysis, an eight-hour expected computation time per "Medium Plant" regime run and an expected computation time of multiple hours per "Small Plant" run had to be avoided. The way to achieve this was to use a warm-start approach, where the solution of the most similar previous run was used as a starting point for the next run. Much faster run times were observed when using this approach, with most of the runs taking less than 30 minutes to complete. However, some "Medium Plant" runs still took almost eight hours and were manually interrupted. Another way to reduce the computation time would be to use heuristics to find good initial solutions, but this was not implemented, as it was not the focus of this work.

This warm start approach was responsible for making many of the runs use the same values for the infrastructure-defining decision variables (i.e., $\dot{m}_{\mathrm{NH}_3,c}$ and y_c) and, for that reason, the complement of the normalized root mean square error was calculated between the different runs to verify how different the solutions were from the business as usual (BAU) scenario. This is a

metric designed to quantify how similar two solutions are, with a value of 1 meaning that the solutions are identical and a value close to 0 meaning that the solutions are very different (for the infrastructure-defining decision variables). The formula used to calculate this metric for each run r is shown below:

$$1 - \text{NRMSE}_r = 1 - \sqrt{\frac{1}{|L_c|} \sum_{c \in L_c} \left[\left(\frac{y_c^r - y_c^{\text{BAU}}}{\mathscr{N}_{\text{max ob.}} - 0} \right)^2 + \left(\frac{\dot{m}_{\text{NH}_3,c}^r - \dot{m}_{\text{NH}_3,c}^{\text{BAU}}}{\dot{m}_{\text{NH}_3,\text{max ob.}} - 0} \right)^2 \right]}, \tag{3.32}$$

where $\mathscr{N}_{\text{max ob.}}$ is the maximum observed number of plants chosen to be built in a single municipality for the regime being analyzed (1 for the "Medium Plant" regime and 3 for the "Small Plant" regime) and $\dot{m}_{\text{NH}_3,\text{max ob.}}$ is the maximum production capacity observed for a single plant in the system. The suffixes r and BAU refer to the run being analyzed and the business as usual scenario, respectively.

Source: Author, based on RODDA; LITTLE (2015).

4 RESULTS

4.1 Parameter Values

The parameter values used in this work were taken from the literature, as shown in Table 4.1.

Table 4.1: Parameter values found and used

Symbol	Units	Range of Values	Used Value	References
$\eta_{\text{H-B}}$	-	97 - 98%	97%	(The. . . , 2023), (HERA et al., 2024), (SHETTY; SANKANNAVAR, 2024)
t_0	-	-	2026	
t_f	-	2046 - 2056	2050[1]	(POZO; SAUMA; BOLADO-LAVíN, 2025; ÖZCAN; KıLıç; ÇELIK, 2025; ONAT; DEMIR, 2025)
$\theta^{\text{MAI}}_{\text{N}_2,\text{air}}$	$\frac{\text{kg of N}_2}{\text{kg of air}}$	0.1510534 - 0.3021068	0.2265801	See Annex A.1
$\theta^{\text{MAI}}_{\text{O}_2,\text{air}}$	$\frac{\text{kg of O}_2}{\text{kg of air}}$	0.0927124 - 0.1390686	0.1158905	See Annex A.2
Q_{el}	$\frac{\text{kWh}}{\text{kg of H}_2}$	33.82 - 39.91	33.82[2]	(HERMESMANN; MüLLER, 2022)

Continued on next page

[1] Each part of the system has a different lifespan. Most critical parts have a longer lifespan.
[2] Using the value for LHV (see Section 2.1.1.4), (NAMI; HENDRIKSEN; FRANDSEN, 2024)

Table 4.1 – continued from previous page

Symbol	Units	Range of Values	Used Value	References
η_{el}^{el}	-	1.40 - 1.60	1.40[3]	(HUANG et al., 2025; HERMESMANN; MüLLER, 2022; Pacific Northwest National Laboratory (PNNL), U.S. DOE Hydrogen and Fuel Cell Technologies Office, 2025)
M_{H_2}	$\frac{g}{mol}$	-	2.01588	(LINSTROM; MALLARD, 2024a)
M_{O_2}	$\frac{g}{mol}$	-	31.9988	(LINSTROM; MALLARD, 2024c)
M_{H_2O}	$\frac{g}{mol}$	-	18.0153	(LINSTROM; MALLARD, 2024d)
M_{N_2}	$\frac{g}{mol}$	-	28.0134	(LINSTROM; MALLARD, 2024b)
η_{el}^{m}	-	89.37 - 98.21%	93.79%	See Annex A.3
$\rho_{PV,c}$	$\frac{kW}{m^2}$	0.1914 - 0.2215	-	(LABREN — Laboratório de Modelagem e Estudos de Recursos Renováveis de Energia; CCST — Centro de Ciência do Sistema Terrestre; INPE — Instituto Nacional de Pesquisas Espaciais, 2017)
η_{PV}	-	20 - 25%	23%	(GREEN et al., 2024)

Continued on next page

[3] Assumed lower end for this range because the plants are going to be built in state-of-the-art modern technology

Table 4.1 – continued from previous page

Symbol	Units	Range of Values	Used Value	References
C_{PV}	$\frac{US\$_{t_0}}{m^2}$	98 - 175	130	(RENAUDINEAU et al., 2025; AZIZI-MONFARED; GHANBARISABAGH, 2026; Empresa de Pesquisa Energética (EPE), 2022)
$\mathcal{N}$	-	-	1 - 5	See Section 3.4.1.4
$\dot{m}_{NH_3,\,min}$	$\frac{\text{tonnes of } NH_3}{day}$	-	10	See Section 3.4.1.4
$\dot{m}_{NH_3,\,max}$	$\frac{\text{tonnes of } NH_3}{day}$	-	100 - 500	See Section 3.4.1.4
$C^{CAPEX}_{H\text{-}B,\,min}$	$US\$_{t_0}$	-	3,753,800.00	See Annex A.5
$C^{CAPEX}_{el,\,min}$	$US\$_{t_0}$	-	2,527,230.46	See Annex A.4
k	-	-	0.65	(LIN; WIESNER; MALMALI, 2020)
FC_{PV}	-	-	3.8%	(RENAUDINEAU et al., 2025)
FC_{el}	-	-	3.7%	(RENAUDINEAU et al., 2025)
$FC_{H\text{-}B}$	-	-	4%	(MERSCH et al., 2024)
i	-		15%	See Section 3.4.1.3
Δ_{c_1,c_2}	km	-	-	See Annex A.6
δ	-	1.2 - 1.5	1.4	(GONçALVES et al., 2014; GIACOMIN; LEVINSON, 2015)
C^{log}	$\frac{US\$_{t_0}}{tonne \cdot km}$	0.05 - 0.2	0.1	See Annex A.8
P^{O_2}	$\frac{US\$_{t_0}}{\text{tonne of } O_2}$	-	200.60	See Annex A.7
$D^{NH_3}_{c,t}$	tonnes of NH_3	-	-	See Section 3.4.1.1
$D^{O_2}_{c,t}$	tonnes of O_2	-	-	See Section 3.4.1.2

4.2 Model Results

4.2.1 Cost breakdown and LCOA

The cost breakdown for the "avg" scenario in both sizing regimes can be seen in Figure 4.1. The figure shows which components contribute the most to the total cost of the system as well as which are most affected by the sizing regime and how much they vary. All the monetary values in this chapter for the OPEX, the logistics costs and the O_2 revenue are in present value (US$ at year t_0).

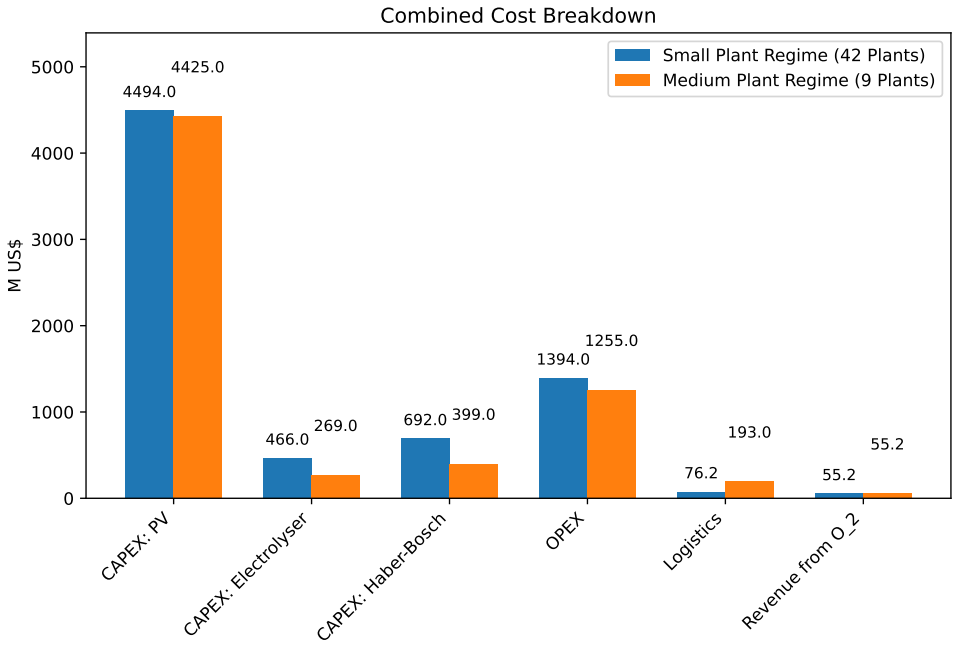

Figure 4.1: Cost breakdown for the "avg" scenario under different plant sizing regimes

As predicted, the "Small Plant" regime has higher costs due to the loss of economies of scale, even though it had lower logistics costs. The CAPEX of the photovoltaic unit is the most significant contributor and had the least variation; this combination is precisely what makes the decentralized system viable.

The following tables show the LCOA for each city in the "avg" scenario and for the whole system for both regimes.

Table 4.2: LCOA - "Small Plant" Regime and "avg" scenario

City	N	Capacity (tonnes/day)	CAPEX (M US$)	OPEX (M US$)	LOGISTICS (M US$)	O_2 Revenue (M US$)	LCOA with O_2 (US$/tonne)	LCOA without O_2 (US$/tonne)
Barra do Bugres	1	100	137.51	33.92	4.77	25.49	555.07	648.93

Continued on next page

Table 4.2 – continued from previous page

City	N	Capacity (tonnes/day)	CAPEX (M US$)	OPEX (M US$)	LOGISTICS (M US$)	O_2 Revenue (M US$)	LCOA with O_2 (US$/tonne)	LCOA without O_2 (US$/tonne)
Brasnorte	1	84.00	120.07	29.62	0.06	0.24	655.51	656.55
Campo Novo do Parecis	1	100	141.05	34.79	0.0	0.21	646.89	647.64
Canarana	1	100	133.95	33.05	0.82	0.29	616.99	618.06
Colíder	1	100	139.24	34.35	3.93	3.39	641.33	653.81
Diamantino	2	200	275.49	67.96	1.74	1.24	644.71	647.04
Feliz Natal	1	100	137.08	33.81	1.29	0.0	742.21	742.21
Itanhangá	1	100	139.51	34.41	2.32	0.0	649.08	649.08
Juína	2	122.75	181.19	44.71	8.35	1.51	783.24	788.33
Lucas do Rio Verde	1	100	138.69	34.21	0.19	0.89	634.19	637.47
Nova Lacerda	1	100	141.31	34.85	3.23	1.37	655.65	660.70
Nova Maringá	1	100	138.84	34.25	1.56	0.0	643.23	643.23
Nova Mutum	2	200	275.92	68.06	1.96	1.28	661.04	663.50
Nova Nazaré	1	100	132.28	32.64	2.86	0.64	854.12	857.37
Nova Ubiratã	2	200	275.14	67.87	0.37	0.01	632.32	632.33
Novo Santo Antônio	1	100	133.17	32.85	2.76	0.0	862.36	862.36
Novo São Joaquim	1	100	132.91	32.79	2.22	0.66	629.71	632.19
Paranatinga	1	100	135.12	33.33	1.26	0.21	624.28	625.05
Planalto da Serra	1	100	135.07	33.32	4.29	0.48	634.26	636.02
Pontal do Araguaia	1	100	133.49	32.93	3.61	1.27	908.85	915.70
Porto dos Gaúchos	1	100	141.77	34.97	0.47	0.96	649.13	652.67
Querência	1	100	135.87	33.52	0.01	0.29	622.78	623.86
Santa Carmem	2	200	276.18	68.13	4.61	2.74	639.94	645.01
Santa Terezinha	1	100	136.37	33.64	5.71	0.79	705.27	708.44
Sapezal	2	200	286.43	70.65	0.44	0.42	657.59	658.36
Sorriso	3	300	414.02	102.13	0.58	2.25	631.60	634.36
São Félix do Araguaia	1	100	134.42	33.16	0.68	0.19	628.23	628.94
São José do Povo	3	300	398.67	98.36	11.11	7.71	614.35	623.81
São José do Rio Claro	1	100	137.53	33.93	1.23	0.13	661.96	662.46
Tapurah	1	100	138.47	34.16	0.08	0.13	635.60	636.07
União do Sul	1	100	137.87	34.01	2.46	0.27	641.12	642.13
Vera	1	100	137.72	33.97	1.27	0.2	636.32	637.05
System	42	4106.75	5652.32	1394.36	76.24	55.25	**656.85**	661.92

Table 4.3: LCOA - “Medium Plant” Regime and “avg” scenario

City	N	Capacity (tonnes/day)	CAPEX (M US$)	OPEX (M US$)	LOGISTICS (M US$)	O_2 Revenue (M US$)	LCOA with O_2 (US$/tonne)	LCOA without O_2 (US$/tonne)
Acorizal	1	500	619.12	152.49	34.52	28.33	572.93	593.80
Campinápolis	1	500	603.14	148.56	27.79	2.73	629.21	631.43
Feliz Natal	1	500	624.96	153.92	17.02	0.34	586.01	586.26
Novo Santo Antônio	1	500	605.42	149.12	25.8	1.27	685.77	686.89
Sorriso	1	500	629.61	155.07	6.13	5.89	578.17	582.51
São José do Povo	1	500	604.03	148.78	23.71	8.04	585.90	592.03
São José do Rio Claro	1	500	627.22	154.48	30.16	2.29	596.33	598.01
Tapurah	1	500	631.91	155.63	25.25	2.07	597.18	598.70
Terra Nova do Norte	1	106.75	147.99	36.5	3.0	4.29	632.04	646.83
System	9	4106.75	5093.39	1254.55	193.37	55.25	**602.80**	607.93

The system LCOA for the “Small Plant” regime is 656.85 US$/tonne (with O_2 revenue) and

for the “Medium Plant” regime is 602.80 US$/tonne (with O_2 revenue). The difference of 54.05 US$/tonne represents an 8.97% increase in LCOA when using the “Small Plant” regime; however, this regime has 42 plants compared to only 9 plants in the “Medium Plant” regime, which can represent a significant advantage in terms of resilience and adaptability to local conditions and is more realistic.

Pistolesi et al. (2025) summarized LCOA values for green ammonia production from various sources, finding values ranging from 395 US$/tonne (in Australia, with solar and wind energy) to 902 US$/tonne (in Denmark, using 100% grid electricity). The result of this work falls within this range, being closer to the higher end.

4.2.2 Location and sizing of the plants

Figure 4.2 shows the location and sizing of the plants for the “avg” scenario.

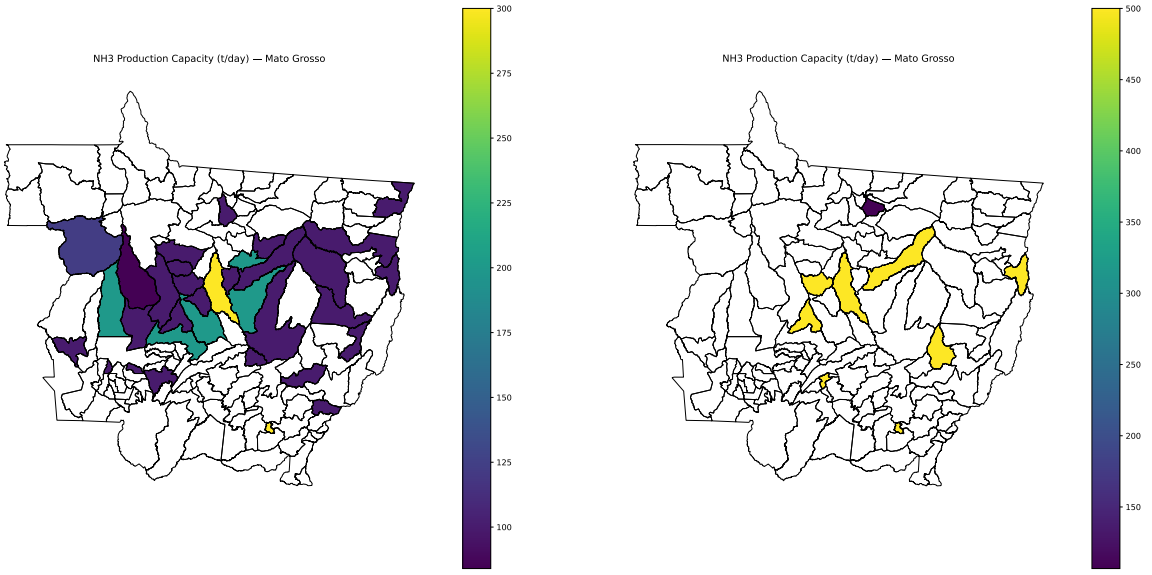

(a) “Small Plant” sizing regime (b) “Medium Plant” sizing regime

Figure 4.2: Location and sizing of the plants for the “avg” scenario

Comparing the result from the “Small Plant” regime to Figures 3.3 and 3.4, it is possible to see that the plants are located very close to the most demanding area of the state, which is expected of a solution that prioritizes decentralization, thus arriving at lower logistics costs. This trend is less clear in the “Medium Plant” regime, where fewer plants are built and thus the location is more influenced by economies of scale, but still a maximum-sized plant is built in the most demanding municipality, Sorriso, and others are built in its vicinity.

Figures 4.3 and 4.4 show the top flows of ammonia both in volume and in cost between

cities.

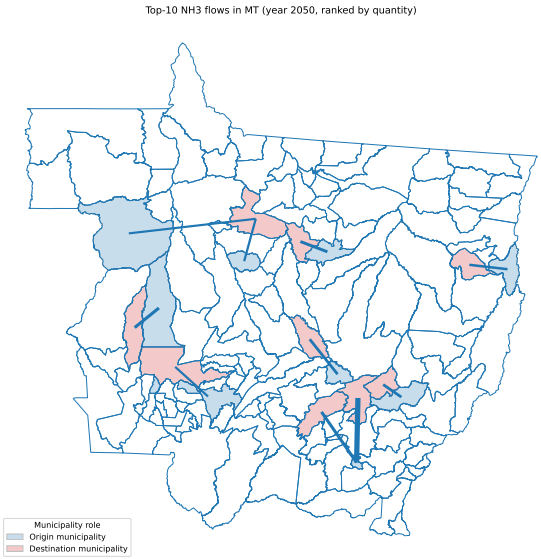

(a) “Small Plant” sizing regime

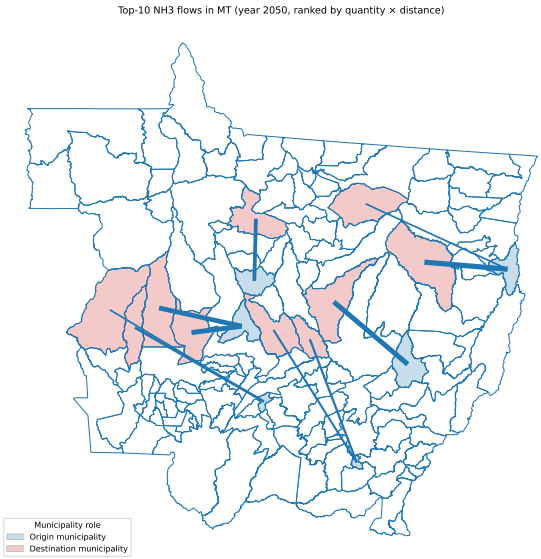

(b) “Medium Plant” sizing regime

Figure 4.3: Top ten flows of ammonia in volume for the “avg” scenario

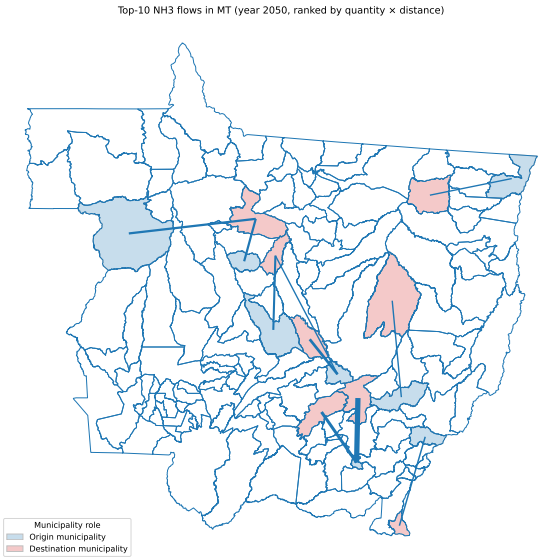

(a) “Small Plant” sizing regime

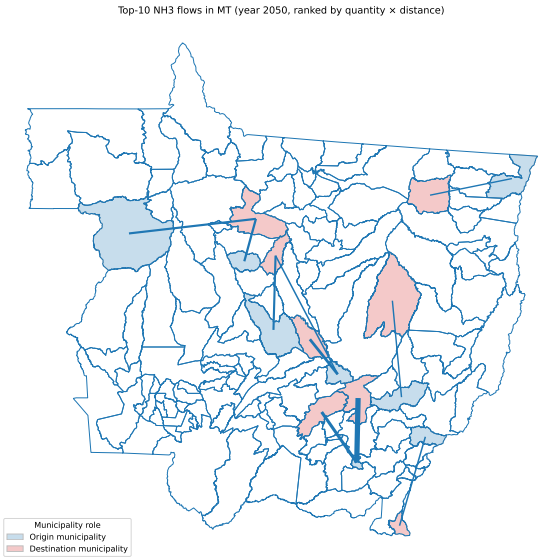

(b) “Medium Plant” sizing regime

Figure 4.4: Top ten flows of ammonia in cost between cities for the “avg” scenario

This set of figures shows that most of the flow of ammonia is between neighboring cities; however, the most costly flows are between cities that are farther apart. This is due to the fact that the logistics cost is proportional to the distance traveled, so even if the volume transported is lower, the cost ends up being higher.

4.3 Sensitivity Analysis

A sensitivity analysis was performed on the economies of scale parameter k, the discount rate i, and the logistics cost factor C^{log}. Also, the "min" and "max" scenarios were analyzed. The results can be seen below. The "gap" column shows the optimality gap of the solution; these gaps were set to be less than or equal to 1%, but the runs that took longer than eight hours were terminated before reaching the desired gap. The "N" column shows the number of plants built in each scenario, and the $1-$NRMSE column shows how similar the values of the infrastructure-defining decision variables (i.e., location and sizing of the plants) are to the business-as-usual run (the "avg" scenario with $k = 0.65$, $i = 15\%$ and $C^{log} = 0.1$ US$/tonne·km), as discussed in Section 3.4.2.

Table 4.4: Sensitivity Analysis Results

Scenario	**Regime**	k	i	C^{log}	**Gap**	**N**	**LCOA (with O_2 Revenue)**	**LCOA (without O_2 Revenue)**	**1 - NRMSE**
"min"	"S. P."	0.65	15%	0.1	≤1%	25	654.57	663.26	83.5%
"min"	"M. P"	0.65	15%	0.1	1.08%	7	603.97	612.66	82.0%
"max"	"S. P."	0.65	15%	0.1	≤1%	60	657.80	661.34	82.7%
"max"	"M. P"	0.65	15%	0.1	≤1%	14	603.58	607.12	83.0%
"avg"	"S. P."	0.60	15%	0.1	≤1%	42	642.32	647.45	100.0%
"avg"	"M. P"	0.60	15%	0.1	≤1%	9	589.40	594.53	98.4%
"avg"	"S. P."	0.70	15%	0.1	≤1%	42	673.15	678.28	100.0%
"avg"	"M. P"	0.70	15%	0.1	≤1%	9	619.27	624.40	100.0%
"avg"	"S. P."	0.65	12.5%	0.1	≤1%	42	590.34	595.46	100.0%
"avg"	"M. P"	0.65	12.5%	0.1	1.37%	9	542.90	548.02	100.0%
"avg"	"S. P."	0.65	17.5%	0.1	≤1%	42	723.30	728.45	100.0%
"avg"	"M. P"	0.65	17.5%	0.1	≤1%	9	662.64	667.79	100.0%
"avg"	"S. P."	0.65	15%	0.085	≤1%	42	655.79	660.92	100.0%
"avg"	"M. P"	0.65	15%	0.085	≤1%	9	600.10	605.24	100.0%
"avg"	"S. P."	0.65	15%	0.115	≤1%	42	657.91	663.05	100.0%
"avg"	"M. P"	0.65	15%	0.115	1.5%	9	605.49	610.63	100.0%
"avg"	"S. P."	0.50	15%	0.1	≤1%	42	617.81	622.94	100.0%
"avg"	"S. P."	0.80	15%	0.1	≤1%	42	711.93	717.06	100.0%
"avg"	"S. P."	0.65	21%	0.1	≤1%	42	814.91	820.08	100.0%
"avg"	"M. P"	0.50	15%	0.1	≤1%	9	568.84	573.97	99.0%
"avg"	"M. P"	0.80	15%	0.1	≤1%	9	663.53	668.67	100.0%
"avg"	"M. P"	0.65	21%	0.1	≤1%	9	745.14	750.32	100.0%

The vertical line in Table 4.4 separates inputs (left) from outputs (right) of the model. In a first moment, only the results above the vertical line were chosen to be calculated due to time constraints; however, after analyzing the results, some additional runs were performed to further explore the sensitivity to extreme values of k and i (the last six lines of the table).

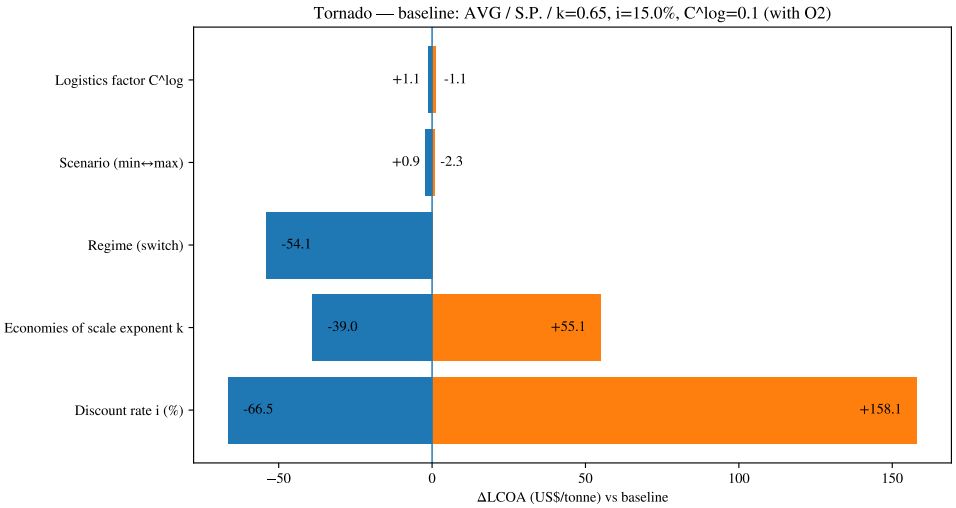

(a) Tornado chart relative to the baseline ("avg", Small Plant, $k = 0.65$, $i = 15\%$, $C^{\log} = 0.1$).

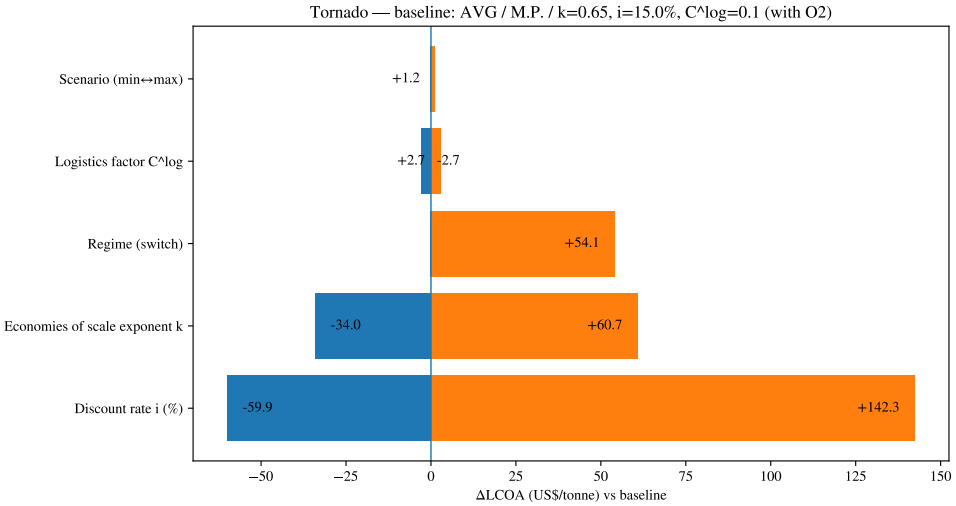

(b) Tornado chart relative to the baseline ("avg", Medium Plant, $k = 0.65$, $i = 15\%$, $C^{\log} = 0.1$).

Figure 4.5: Tornado charts showing the impact on LCOA (US$/tonne) vs. baseline for the main parameters, scenario and regime.

These results show that the location and sizing of the plants presented in Figure 4.2 are extremely robust, since, among the parameters not attached to the demand, only a change in the economies of scale parameter k was able to cause a very minor change in the location and sizing of the plants (and only for the "Medium Plant" regime). Interestingly, changes in the demand scenarios caused significant changes in the location and sizing of the plants, but did not have a great impact on the LCOA, which further emphasizes the adaptability and relevance of this model.

The logistics factor would probably have a greater impact if larger distances were considered; this work focused on a single state, so the distances between cities are relatively small.

Future work could consider a larger area, such as the whole country, which would probably increase the impact of logistics costs on the LCOA and perhaps even on the location and sizing of the plants.

The economies of scale parameter k had a significant impact on the LCOA, which can be expected since it directly affects the CAPEX of the electrolyzer and the Haber–Bosch unit, which are large contributors to the overall cost and among the most volatile components, given that the CAPEX of the photovoltaic system is more influenced by the irradiance of the chosen locations and that the logistics costs are quite small for this scale of analysis. One could expect this parameter to also have a significant impact on the location and sizing of the plants; however, this was only observed for the "Medium Plant" regime, which suggests that the "Small Plant" regime has such a limited maximum size that the variance in the economies of scale effect is not enough to change the optimal sizing and location of the plants (considering a gap of 1%).

The discount rate i also had a significant impact on the LCOA without changing the location and sizing of the plants. This could cause confusion, since the discount rate affects both costs and production over time (as shown in Equation 3.14); however, one should notice that the installed capacity of each plant is constant over time and corresponds to the demand of the last year considered, which is much greater than the demand for the first year (as can be seen in Figure 3.2). The fact that the relationship between LCOA and i appears to be linear (see Figure 4.6b) is also evidence of this behavior. This is inevitable for this model structure and will always lead to higher discounting of production than of costs, given that most costs are upfront (CAPEX) or constant over time (OPEX and logistics), while production starts low and increases over time, leading to a higher sensitivity of the LCOA to the discount rate. Future work could consider investment periods and a salvage factor to represent the capital recovery at the end of the project lifetime to mitigate this effect, and the best results would be found when the discount rate has a very low impact on the LCOA.

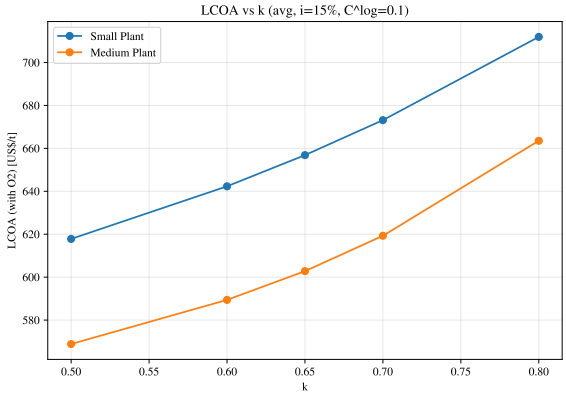

(a) LCOA vs. k (“avg”).

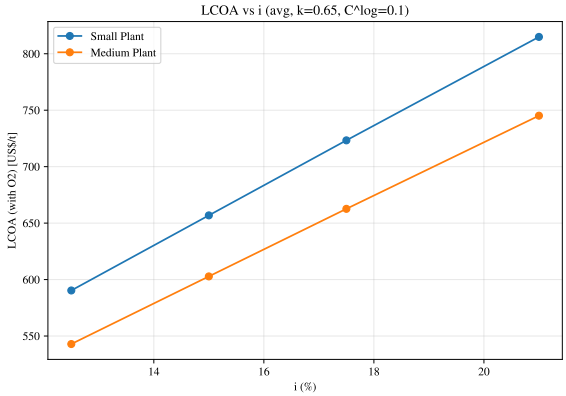

(b) LCOA vs. i (“avg”).

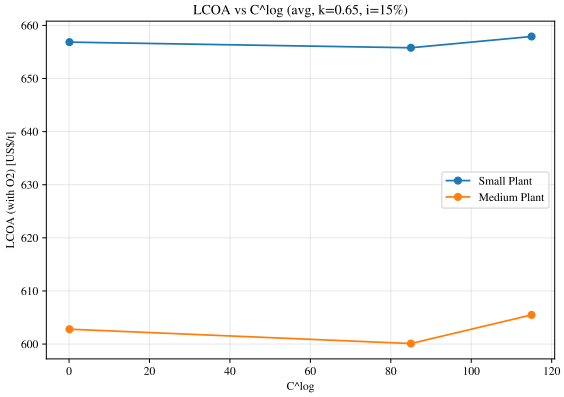

(c) LCOA vs. $C^{\log}$ (“avg”).

Figure 4.6: Sensitivity of LCOA to k, i, and $C^{\log}$ under the “avg” scenario for both regimes.

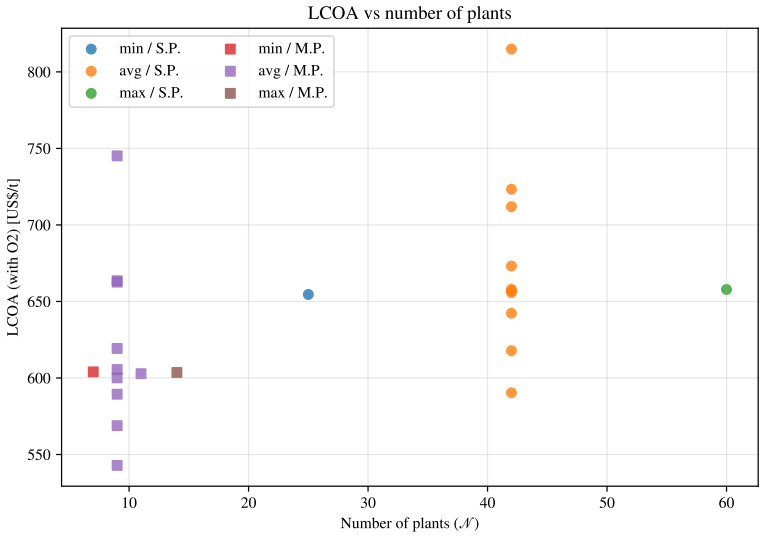

Figure 4.7: LCOA vs. number of plants N across scenarios and regimes.

Figure 4.7 contains all the runs performed in this work, and clearly shows that different parameters affect the LCOA and the number of plants in different ways. This also further empha-

sizes the adaptability of the model to different conditions, since many different configurations of plants can lead to similar LCOA values.

4.4 Discussion of the Results

The results obtained in this work show that the proposed optimization model is able to find suitable locations and sizings for green ammonia production plants that are able to meet the projected demand for the state of Mato Grosso with a competitive LCOA when compared to literature values. The sensitivity analysis shows that the model is robust to changes in the parameters tested, with the location and sizing of the plants remaining largely unchanged across a range of scenarios, as seen by the values of the "1 - NRMSE" column of Table 4.4.

One possible improvement to the model would be to include investment periods, instead of having a single CAPEX at the start of the project. This would allow for a more realistic representation of the investment and cash flow over time, especially for long-term projects where costs and revenues may vary significantly over the lifespan of the plant. With regard to investment costs, including capacity expansion options could drastically reduce LCOA, since in this work demand was considered to peak only around 2030, so there would be a financial advantage in building smaller photovoltaic units at first and expanding them later as demand increases. Another possible improvement would be to include taxes and subsidies, which could have a significant impact on the choice of municipalities for plant installation, as well as on the overall LCOA.

It is also worth to mention that the usage of a simple parameter k to represent economies of scale is a simplification very present in scientific literature, but in practice a more detailed analysis would be performed by a company looking to invest in such a project, considering specific equipment and suppliers to obtain more accurate CAPEX values for each plant size. This approach would require access to more detailed data on prices of equipment and installation costs, and would envolve likely the analysis of multiple scenarios, changing the direct correstpondence between plant size and CAPEX that is present in this work to a pre calculated CAPEX value for each plant size at each location making the problem a Mixed Integer Linear Programming (MILP) one instead of a MINLP but adding way more integer variables. The approach present in this work is still useful to demonstrate economic trends to investors and decision makers, as well as to provide a first estimate of the LCOA for green ammonia production in the region.

It is also worth mentioning that the use of a simple parameter k to represent economies

of scale is a simplification that is very common in the scientific literature, but in practice a more detailed analysis would be performed by a company looking to invest in such a project, considering specific equipment and suppliers to obtain more accurate CAPEX values for each plant size. This approach would require access to more detailed data on equipment prices and installation costs and would likely involve the analysis of multiple scenarios, changing the direct correspondence between plant size and CAPEX that is present in this work to a pre-calculated CAPEX value for each plant size at each location, making the problem a Mixed-Integer Linear Programming (MILP) one instead of a MINLP, but adding many more integer variables. The approach presented in this work is still useful to demonstrate economic trends to investors and decision makers, as well as to provide a first estimate of the LCOA for green ammonia production in the region.

5 CONCLUSION

This work proposed and applied a mathematical programming model to verify the economic viability of the production of green ammonia in Brasil, particularly in the State of Mato Grosso. This goal closely aligns to the government's strategic plans by providing preliminar data on the production of such an important molecule within the most ammonia consuming state with a sustainable and reliable energy source.

The proposed model was used to decide on the location and sizing of multiple green ammonia plants designed to supply the entire fertilizer-related ammonia demand of the state over a multi-decade horizon. The model captures the main steps of a green ammonia supply chain: renewable electricity generation, water electrolysis, membrane air separation, the Haber-Bosch synthesis loop, and the distribution of ammonia and by-product oxygen across municipalities.

Under the baseline "avg" demand scenario and central values for the economies-of-scale exponent and discount rate, the model indicates that viable configurations concentrate plants in and around the main demand hubs, especially Sorriso and neighboring municipalities, while also taking advantage of the relatively homogeneous and favorable solar resource across the state. In the enforced "Small Plant" regime, the optimal solution builds 42 plants, each with capacities up to 100 tonnes/day, distributed so as to reduce transportation distances. In the "Medium Plant" regime, the model selects 9 larger plants, with capacities up to 500 tonnes/day, still anchored around high-demand areas but serving a wider set of municipalities and taking more advantage of economies of scale. For these configurations, the system-level LCOA is 656.85 US$/tonne in the Small Plant regime and 602.80 US$/tonne in the Medium Plant regime, both including O_2 revenue.

Comparing the two sizing regimes shows that enforcing a more distributed configuration through smaller plants and tighter constraints on plant size leads to a clear increase on overall costs because of the loss of economies of scale. While the Small Plant regime achieves lower logistics costs, because plants are more spatially dispersed and closer to demand, the reduction in transportation expenditure is not sufficient to compensate for the increase in capital and operating costs associated with multiple small units. As a result, the baseline LCOA in the Small

Plant regime is roughly 9% higher than in the Medium Plant regime. This result highlights that, under the cost assumptions adopted here, moderate centralization of production at a limited number of medium-sized plants is economically preferable to enforcing strict decentralization, at least when only road transport and plant-level economies of scale are considered. However, this may not be the case when studying the whole country and other factors not included in this work's cost appreciations, such as, labour costs and opportunities and government subsidies.

The sensitivity analysis shows that the discount rate and the economies of scale exponent are the dominant drivers of variation in LCOA between the analyzed parameters. Changes in the discount rate within plausible bounds lead to substantial shifts in LCOA, reflecting the long-lived and capital-intensive nature of green ammonia projects. Likewise, varying the economies of scale exponent k significantly affects LCOA. In contrast, realistic variations in the logistics cost factor and in the spatial distribution of demand have almost no impact on LCOA, even though demand scenarios do influence the number of plants built and, to a lesser extent, their placement. Importantly, the 1 - NRMSE metric indicates that the infrastructure-defining decision variables (locations and sizes) remain highly similar to the baseline configuration across most parameter variations, with noticeable structural changes occurring only for more extreme values of k or when evaluating different demand scenarios. Overall, this suggests that the system's optimal configuration is relatively robust, whereas its economic viability is strongly contingent on financing conditions and on the realization of economies of scale.

Finally, across all scenarios and regimes, the revenue from selling by-product oxygen plays a secondary but non-negligible role: it reduces LCOA by approximately 5 US$/tonne in the baseline cases, without altering the qualitative conclusions about optimal locations and plant sizes. This might be more pronounced in states that have more and more geographically distributed hospital beds.

5.1 Limitations and Future Work

As with any modeling exercise, the results presented here are subject to important limitations. First, investment decisions are modeled as a single-stage problem: all plants are assumed to be built at the beginning of the planning horizon, and the model does not consider phased expansions, plant decommissioning or even the time needed to construct them. Allowing for multi-period investment decisions would provide a more realistic representation of how enterprises actually deploy capital under demand uncertainty and evolving technology costs. Second, economies of scale are represented via a single exponent k applied to aggregate plant capacity, rather than through detailed equipment-level cost correlations. While this choice enables

tractability and captures the general trend of decreasing average cost with scale, it abstracts away from specific design choices that could be important in practice.

Third, the model does not explicitly incorporate taxes, subsidies, carbon credits, or other regulatory instruments that are likely to play a decisive role in the deployment of green ammonia projects in Brazil. The resulting LCOA should therefore be interpreted as a pre-policy techno-economic benchmark rather than as an exact prediction of market prices or project profitability. Finally, the logistics representation is restricted to road transport between municipalities, with a single logistics cost factor and a fixed circuity factor; other transport modes and more detailed network characteristics could alter the relative attractiveness of different locations, especially when extending the analysis beyond a single state.

REFERENCES

AZIZ, M.; TRIWIJAYANTA, A.; NANDIYANTO, A. B. D. Ammonia as effective hydrogen storage: A review on production, storage and utilization. *Energies*, v. 13, n. 12, 2020. Cited by: 449; All Open Access, Gold Open Access, Green Open Access.

AZIZI-MONFARED, H.; GHANBARISABAGH, M. Hybrid intelligent control and maximum power point tracking of a solar generator under variable irradiance and temperature using a multi-method approach. *International Journal of Engineering*, Materials and Energy Research Center, v. 39, n. 6, p. 1462–1481, 2026. ISSN 1025-2495.

BAKER, R. W. *Membrane technology and applications*. [S.l.]: John Wiley & Sons, 2023.

BASTOS, J. L. M. et al. *Custos de Transporte e Valor do Tempo para Cargas*. [S.l.], 2024. Plano Nacional de Logística (PNL).

BOZORG, M. et al. Polymeric membrane materials for nitrogen production from air: A process synthesis study. *Chemical Engineering Science*, v. 207, p. 1196 – 1213, 2019. Cited by: 50; All Open Access, Bronze Open Access, Green Open Access.

BRANKER, K.; PATHAK, M. J. M.; PEARCE, J. M. A review of solar photovoltaic levelized cost of electricity. *Renewable and Sustainable Energy Reviews*, v. 15, n. 9, p. 4470 – 4482, 2011.

Brasil. Ministério da Saúde. Departamento de Atenção Hospitalar, Domiciliar e de Urgência (DAHU). Coordenação-Geral de Atenção Hospitalar e Domiciliar (CGHID). *Hospitais e Leitos — Leitos 2025*. [S.l.]: OpenDataSUS — Ministério da Saúde (Brasil), 2025. Fonte: CNES. Licença: Creative Commons Atribuição.

BROWN, T.; REICHENBERG, L. Decreasing market value of variable renewables can be avoided by policy action. *Energy Economics*, v. 100, p. 105354, 2021.

CARMO, M. et al. A comprehensive review on pem water electrolysis. *International Journal of Hydrogen Energy*, v. 38, n. 12, p. 4901 – 4934, 2013. Cited by: 4127.

CEKIRGE, H. M.; ERTURAN, S. Modified levelized cost of electricity or energy (mlcoe) and modified levelized avoided cost (mlace) and decision making. *American Journal of Modern Energy*, v. 5, n. 1, p. 1 – 4, 2019.

DASKIN, M. S. Book. *Network and Discrete Location Models, Algorithms, and Applications*. [S.l.: s.n.], 2013. 1 – 516 p. Cited by: 1201.

DREZNER, Z.; HAMACHER, H. W. *Facility location: applications and theory*. [S.l.]: Springer Science & Business Media, 2004.

DUTENKEFER, R. d. M. et al. Brazilian municipal ammonia demand estimates. Provided to the author on 2025-09-15; cited with permission; part of the Petronas Research Project. 2025.

ECONOMIC Indicators: CE Plant Cost Index (Annual Index). 2024. Chemical Engineering magazine (PDF of monthly Economic Indicators pages). Annual Index list includes 2020 = 596.2 (base 1957–59 = 100) and 2023 = 797.9.

EMBLEMSVåG, J. Rethinking the "levelized cost of energy": A critical review and evaluation of the concept. *Energy Research and Social Science*, v. 119, 2025. Cited by: 8; All Open Access, Hybrid Gold Open Access.

Empresa de Pesquisa Energética (EPE). *Power Generation Costs Report 2021*. Rio de Janeiro, Brazil, 2022. Revision r1 of report EPE-DEE-RE-089/2021.

FRIEDL, G. et al. Applications of the levelized cost concept. *Journal of Business Economics*, v. 93, n. 6, p. 1125 – 1148, 2023.

GARCIA, V. F.; PALACIOS, R.; ENSINAS, A. Optimisation of ammonia production and supply chain from sugarcane ethanol and biomethane: A robust mixed-integer linear programming approach. *Processes*, v. 12, n. 10, 2024.

GARDINER, M. *Energy requirements for hydrogen gas compression and liquefaction as related to vehicle storage needs*. Washington, D.C., 2009. Approved by Sunita Satyapal on October 26, 2009.

GIACOMIN, D. J.; LEVINSON, D. M. Road network circuity in metropolitan areas. *Environment and Planning B: Planning and Design*, v. 42, n. 6, p. 1040 – 1053, 2015. Cited by: 56.

GONçALVES, D. N. S. et al. Analysis of the difference between the euclidean distance and the actual road distance in brazil. *Transportation Research Procedia*, v. 3, p. 876–885, 2014. ISSN 2352-1465. 17th Meeting of the EURO Working Group on Transportation, EWGT2014, 2-4 July 2014, Sevilla, Spain.

GREEN, M. A. et al. Solar cell efficiency tables (version 64). *Progress in Photovoltaics: Research and Applications*, v. 32, n. 7, p. 425 – 441, 2024. Cited by: 489; All Open Access, Gold Open Access, Green Open Access.

Gurobi Optimization, LLC. *Gurobi Optimizer Reference Manual*. 2025.

GóMEZ-CHAPARRO, M.; GARCíA-SANZ-CALCEDO, J.; MáRQUEZ, L. A. Analytical determination of medical gases consumption and their impact on hospital sustainability. *Sustainability (Switzerland)*, v. 10, n. 8, 2018. Cited by: 24; All Open Access, Gold Open Access, Green Open Access.

HASSAN, Q. et al. A review of hybrid renewable energy systems: Solar and wind-powered solutions: Challenges, opportunities, and policy implications. *Results in Engineering*, v. 20, 2023. Cited by: 248; All Open Access, Gold Open Access.

HELMEISTER, M. C. *ANALYSIS UNDER UNCERTAINTY OF THE LEVELIZED COST OF HYDROGEN PRODUCED BY AMMONIA DECOMPOSITION*. 2024. Trabalho de Conclusão de Curso (Graduação) - Escola Politécnica, Universidade de São Paulo.

HERA, G. de la et al. Flexible green ammonia production plants: Small-scale simulations based on energy aspects. *Environments - MDPI*, v. 11, n. 4, 2024. Cited by: 6; All Open Access, Gold Open Access, Green Open Access.

HERMESMANN, M.; MüLLER, T. Green, turquoise, blue, or grey? environmentally friendly hydrogen production in transforming energy systems. *Progress in Energy and Combustion Science*, v. 90, 2022. Cited by: 425.

HIGNETT, T. P. Transportation and storage of ammonia. In: ____. *Fertilizer Manual*. Dordrecht: Springer Netherlands, 1985. p. 73 – 82. ISBN 978-94-017-1538-6. Disponível em: ⟨10.1007/978-94-017-1538-6_7⟩.

HUANG, C. et al. A review of alkaline electrolyzer technology modeling and applications for decision-making optimization in energy systems. *Renewable and Sustainable Energy Reviews*, v. 224, 2025. Cited by: 0; All Open Access, Hybrid Gold Open Access.

HUBERT, M. et al. *Clean Hydrogen Production Cost Scenarios with PEM Electrolyzer Technology*. [S.l.], 2024.

IBGE. *Consumo aparente de matérias-primas para fertilizantes*. [S.l.], 2023.

IBGE. *Tabela 5457 - Área plantada ou destinada à colheita, área colhida, quantidade produzida, rendimento médio e valor da produção das lavouras temporárias e permanentes*. [S.l.], 2025.

IDEL, R. Levelized full system costs of electricity. *Energy*, v. 259, p. 124905, 2022.

IEA; NEA. *Projected Costs of Generating Electricity 2020*. [S.l.]: OECD Publishing, 2020. Includes the VALCOE framework.

IEAGHG. *Beyond LCOE: Accounting for the Value and System Effects of Low-Carbon Power*. [S.l.], 2020.

Instituto Produzir, Conservar e Incluir (PCI). *Trajetória PCI: Produzir, Conservar e Incluir de 2015 a 2022 – Avanços na maior iniciativa de sustentabilidade jurisdicional do país*. Cuiabá, MT, 2022. Relatório de atividades.

International Energy Agency. *Projected Costs of Generating Electricity 2020: Annex on Value-Adjusted LCOE (VALCOE)*. [S.l.], 2020. VALCOE methodology overview.

International Energy Agency. *Global Energy and Climate Model Documentation 2024*. Paris, 2024. See Section 4.2 “Value-adjusted Levelised Cost of Electricity (VALCOE)”, pp. 54–57.

International Energy Agency (IEA). [S.l.], 2025.

JOSKOW, P. L. Comparing the costs of intermittent and dispatchable electricity generating technologies. *American Economic Review*, v. 101, n. 3, p. 238 – 241, 2011.

KABEYI, M. J. B.; OLANREWAJU, O. A. The levelized cost of energy and modifications for use in electricity generation planning. *Energy Reports*, v. 9, p. 495–534, 2023. ISSN 2352-4847. Technologies and Materials for Renewable Energy, Environment and Sustainability.

KHAKSAR, S. A. N.; RAHIMPOUR, H. R.; RAHIMPOUR, M. R. Book chapter. *Ammonia storage and transportation*. [S.l.: s.n.], 2024. 251 - 270 p. Cited by: 7.

KLERKE, A. et al. Ammonia for hydrogen storage: Challenges and opportunities. *Journal of Materials Chemistry*, v. 18, n. 20, p. 2304 – 2310, 2008. Cited by: 1132.

KUMAR, S. S.; HIMABINDU, V. Hydrogen production by pem water electrolysis - a review. *Materials Science for Energy Technologies*, v. 2, n. 3, p. 442 – 454, 2019. Cited by: 1840; All Open Access, Gold Open Access.

LABREN — Laboratório de Modelagem e Estudos de Recursos Renováveis de Energia; CCST — Centro de Ciência do Sistema Terrestre; INPE — Instituto Nacional de Pesquisas Espaciais. *Atlas Brasileiro de Energia Solar: Base de Dados (2^a edição, 2017)*. São José dos Campos, SP, Brasil, 2017.

LAGARINHOS, C. A. F.; AZEVEDO, L. P. Book chapter. *Challenges and opportunities of hydrogen economy in Industrial Revolution 4.0 era*. [S.l.: s.n.], 2024. 237 - 256 p.

LAPORTE, G.; NICKEL, S.; GAMA, F. S. da. Book. *Location Science*. [S.l.: s.n.], 2015. 1 – 644 p. Cited by: 265.

LEAL, F. I.; REGO, E. E.; RIBEIRO, C. de O. Levelized cost analysis of thermoelectric generation in brazil: A comparative economic and policy study with environmental implications. *Journal of Natural Gas Science and Engineering*, v. 44, p. 191 – 201, 2017. Cited by: 15.

LIN, B.; WIESNER, T.; MALMALI, M. Performance of a small-scale haber process: A techno-economic analysis. *ACS Sustainable Chemistry and Engineering*, v. 8, n. 41, p. 15517 – 15531, 2020. Cited by: 100.

LINSTROM, P. J.; MALLARD, W. G. *Hydrogen, H_2: Molecular Weight and Thermochemical Data*. [S.l.]: National Institute of Standards and Technology, 2024. NIST Chemistry WebBook, NIST Standard Reference Database Number 69.

LINSTROM, P. J.; MALLARD, W. G. *Nitrogen, N_2: Molecular Weight and Thermochemical Data*. [S.l.]: National Institute of Standards and Technology, 2024. NIST Chemistry WebBook, NIST Standard Reference Database Number 69.

LINSTROM, P. J.; MALLARD, W. G. *Oxygen, O_2: Molecular Weight and Thermochemical Data*. [S.l.]: National Institute of Standards and Technology, 2024. NIST Chemistry WebBook, NIST Standard Reference Database Number 69.

LINSTROM, P. J.; MALLARD, W. G. *Water, H_2O: Molecular Weight and Thermochemical Data*. [S.l.]: National Institute of Standards and Technology, 2024. NIST Chemistry WebBook, NIST Standard Reference Database Number 69.

LTD, A. A. P. *Water for Hydrogen: Technical Paper*. Brisbane, QLD, Australia, 2022. Reviewed by CSIRO.

LUECKEL, F. B. B.; MONAGHAN, R. F.; LYNCH, M. A. Hydrogen supply chain modelling at energy system scale: A review. *Renewable and Sustainable Energy Reviews*, v. 210, 2025. Cited by: 5; All Open Access, Green Open Access.

MANHAS, V. et al. Cost analysis of different medical oxygen sources for a healthcare facility in india. *Indian Journal of Anaesthesia*, v. 68, n. 4, p. 374 – 379, 2024. Cited by: 5; All Open Access, Gold Open Access, Green Open Access.

MANZOLINI, G. et al. An economic index to overcome levelized cost of electricity limitations. *iScience*, v. 27, n. 6, p. 109897, 2024.

MATSUO, Y. Re-defining the system lcoe to evaluate renewable integration costs. *Energies*, v. 15, n. 22, p. 8284, 2022.

MCCAMY, C. S. *A Survey of the Hazards of Handling Liquid Oxygen*. Washington, DC, 1956. “In the gaseous state, at 0°C and 760 mm Hg, oxygen has a density of 1.429 g/L.”.

MERSCH, M. et al. A comparative techno-economic assessment of blue, green, and hybrid ammonia production in the united states. *Sustainable Energy and Fuels*, 2024. Cited by: 22; All Open Access, Hybrid Gold Open Access.

Ministério da Ciência, Tecnologia e Inovação. *Fator de emissão de CO2 na geração de energia elétrica no Brasil em 2023 é o menor em 12 anos*. [S.l.], 2024.

Ministério da Indústria, Comércio Exterior e Serviços. *Plano Nacional de Fertilizantes 2050*. [S.l.], 2023.

MITRAI, I.; PALYS, M. J.; DAOUTIDIS, P. A two-stage stochastic programming approach for the design of renewable ammonia supply chain networks. *Processes*, v. 12, n. 2, p. 325, 2024.

NADALETI, W. C. et al. Hydrogen and electricity potential generation from rice husks and persiculture biomass in rio grande do sul, brazil. *Renewable Energy*, v. 216, 2023. Cited by: 4.

NAMI, H.; HENDRIKSEN, P. V.; FRANDSEN, H. L. Green ammonia production using current and emerging electrolysis technologies. *Renewable and Sustainable Energy Reviews*, v. 199, p. 114517, 2024. ISSN 1364-0321.

NAYAK-LUKE, R. M.; BAñARES-ALCáNTARA, R. Techno-economic viability of islanded green ammonia as a carbon-free energy vector and as a substitute for conventional production. *Energy and Environmental Science*, v. 13, n. 9, p. 2957 – 2966, 2020. Cited by: 148; All Open Access, Green Open Access, Hybrid Gold Open Access.

NICOLETTI, G. et al. A technical and environmental comparison between hydrogen and some fossil fuels. *Energy Conversion and Management*, v. 89, p. 205 – 213, 2015. Cited by: 451.

NIST Physical Measurement Laboratory. *Composition of AIR, DRY near sea level*. Online. Compositions of Materials used in STAR Databases. Accessed: 2025-10-03.

NYANGON, J.; DAREKAR, A. Advancements in hydrogen energy systems: A review of levelized costs, financial incentives and technological innovations. *Innovation and Green Development*, v. 3, n. 3, p. 100149, 2024. ISSN 2949-7531.

ONAT, M. R.; DEMIR, M. E. Techno-economic assessment of green ammonia and hydrogen distribution from offshore wind farms to european ports. *International Journal of Hydrogen Energy*, v. 142, p. 1272–1286, 2025. ISSN 0360-3199.

Pacific Northwest National Laboratory (PNNL), U.S. DOE Hydrogen and Fuel Cell Technologies Office. Online, *Hydrogen Density at Different Temperatures and Pressures*. 2025. Provides tabulated hydrogen gas density versus temperature and pressure (includes near-STP values).

PANIGRAHI, P. K. et al. Potential benefits, challenges and perspectives of various methods and materials used for hydrogen storage. *Energy and Fuels*, v. 38, n. 4, p. 2630 – 2653, 2024. Cited by: 39.

PAVAN, F. et al. *Hydrogen*. [S.l.], 2025.

PINSKY, R. et al. Comparative review of hydrogen production technologies for nuclear hybrid energy systems. *Progress in Nuclear Energy*, v. 123, 2020. Cited by: 266; All Open Access, Bronze Open Access.

PISTOLESI, C. et al. Flexible green ammonia production: Impact of process design on the levelized cost of ammonia. *Fuels*, MDPI, v. 6, n. 2, p. 39, 2025.

POZO, D.; SAUMA, E.; BOLADO-LAVíN, R. Levelized cost analysis for renewable ammonia production in chile. *Energy*, v. 335, 2025. Cited by: 0; All Open Access, Hybrid Gold Open Access.

PREUSTER, P.; PAPP, C.; WASSERSCHEID, P. Liquid organic hydrogen carriers (lohcs): Toward a hydrogen-free hydrogen economy. *Accounts of Chemical Research*, v. 50, n. 1, p. 74 – 85, 2017. Cited by: 854.

RAVI, M.; MAKEPEACE, J. W. Facilitating green ammonia manufacture under milder conditions: What do heterogeneous catalyst formulations have to offer? *Chemical Science*, v. 13, n. 4, p. 890 – 908, 2022. Cited by: 67; All Open Access, Gold Open Access, Green Open Access.

RENAUDINEAU, H. et al. Green hydrogen production from off-grid photovoltaic: An assessment on optimal sizing. *Renewable Energy*, v. 246, 2025. Cited by: 4.

RIERA, J. A.; LIMA, R. M.; KNIO, O. M. A review of hydrogen production and supply chain modeling and optimization. *International Journal of Hydrogen Energy*, v. 48, n. 37, p. 13731–13755, 2023.

RODDA, H. J. E.; LITTLE, M. A. *Understanding Mathematical and Statistical Techniques in Hydrology: An Examples-Based Approach*. Oxford: Wiley-Blackwell, 2015. ISBN 9781444335491.

SALMON, N.; BAñARES-ALCáNTARA, R. Green ammonia as a spatial energy vector: A review. *Sustainable Energy and Fuels*, v. 5, n. 11, p. 2814 – 2839, 2021. Cited by: 217; All Open Access, Green Open Access, Hybrid Gold Open Access.

SANTOS, M. et al. Biogas, hydrogen, green ammonia and electricity production from canned peach processing residues: Aspects of the circular economy for the brazilian agroindustry. *International Journal of Hydrogen Energy*, v. 105, p. 45 – 55, 2025. Cited by: 0.

SHETTY, A. U.; SANKANNAVAR, R. Exploring nitrogen reduction reaction mechanisms in electrocatalytic ammonia synthesis: A comprehensive review. *Journal of Energy Chemistry*, v. 92, p. 681–697, 2024. ISSN 2095-4956.

SHORT, W.; PACKEY, D.; HOLT, T. *A Manual for the Economic Evaluation of Energy Efficiency and Renewable Energy Technologies*. 1995.

SIMOES, S. G. et al. Water availability and water usage solutions for electrolysis in hydrogen production. *Journal of Cleaner Production*, v. 315, p. 128124, 2021. ISSN 0959-6526.

SKIPPER, S.; JOSEF, P. statsmodels. *9th Python in Science Conference*, 2010.

STABILE, M. C. et al. Solving brazil's land use puzzle: Increasing production and slowing amazon deforestation. *Land Use Policy*, v. 91, 2020. Cited by: 161; All Open Access, Hybrid Gold Open Access.

SUN, E. et al. Thermodynamic study of semi-closed rankine cycle based on direct combustion of hydrogen fuel. *International Journal of Hydrogen Energy*, v. 92, p. 1463–1475, 2024. ISSN 0360-3199.

SVENSSON, G. E. with S. *EU rules for renewable hydrogen Delegated regulations on a methodology for renewable fuels of non-biological origin*. 2023. Briefing.

TELLO, A. et al. Green hydrogen production by photovoltaic-assisted alkaline water electrolysis: A review on the conceptualization and advancements. *International Journal of Hydrogen Energy*, v. 107, p. 378 – 395, 2025. Cited by: 7.

The Haber Process. [S.l.]: Truro School in Cornwall, 2023. [Online; accessed 2025-07-01].

TIMILSINA, G. R. *Are Renewable Energy Technologies Cost Competitive for Electricity Generation?* [S.l.], 2020.

UECKERDT, F. et al. System lcoe: What are the costs of variable renewables? *Energy*, v. 63, p. 61 – 75, 2013.

U.S. Energy Information Administration. *Levelized Cost of Electricity and Levelized Avoided Cost of Electricity Methodology Supplement*. [S.l.], 2013.

U.S. Energy Information Administration. *Levelized Cost of New Generation Resources in the* Annual Energy Outlook. [S.l.], 2023.

WAN, Z. et al. Ammonia as an effective hydrogen carrier and a clean fuel for solid oxide fuel cells. *Energy Conversion and Management*, Elsevier Ltd, v. 228, n. 113729, 2021.

WIJAYANTA, A. T. et al. Liquid hydrogen, methylcyclohexane, and ammonia as potential hydrogen storage: Comparison review. *International Journal of Hydrogen Energy*, v. 44, n. 29, p. 15026–15044, 2019. ISSN 0360-3199.

YUE, M. et al. Hydrogen energy systems: A critical review of technologies, applications, trends and challenges. *Renewable and Sustainable Energy Reviews*, v. 146, 2021. Cited by: 1359; All Open Access, Green Open Access, Hybrid Gold Open Access.

ÖZCAN, H.; KıLıç, A. E.; ÇELIK, S. Comparative techno-economic assessment of small-scale e-haber-bosch, plasma-electrocatalytic, and direct electrochemical nitrogen reduction pathways for clean and decentralized ammonia production. *Journal of Cleaner Production*, v. 524, p. 146473, 2025. ISSN 0959-6526.

ANNEX A – PARAMETER ESTIMATION

A.1 $\theta^{\mathbf{MAI}}_{\mathbf{N_2,air}}$

Assumptions:

- Dry air is composed of 75.5267% N_2 and 23.1781% O_2 by mass (NIST Physical Measurement Laboratory,).
- $\theta^{\mathrm{MAI}}_{\mathrm{N_2,air}}$ is proportional to the mass fraction of N_2 in dry air. (BAKER, 2023)
- The fraction between $\theta^{\mathrm{MAI}}_{\mathrm{N_2,air}}$ and the mass fraction of N_2 in dry air is varies according to the purity of N_2 in the MAI output stream.
- The MAI output stream will be set to have a N_2 purity of 99.9% to feed the H-B synthesis loop with high-purity N_2.
- For this purity, the fraction between $\theta^{\mathrm{MAI}}_{\mathrm{N_2,air}}$ and the mass fraction of N_2 in dry air has to be assumed to be in the lower range of possible values, between 0.2 and 0.4. (BOZORG et al., 2019)

Therefore, $\theta^{\mathrm{MAI}}_{\mathrm{N_2,air}} = 0.755267 \times 0.2$ to $0.755267 \times 0.4 = 0.1510534$ to 0.3021068.

A.2 $\theta^{\mathbf{MAI}}_{\mathbf{O_2,air}}$

The same model used for $\theta^{\mathrm{MAI}}_{\mathrm{N_2,air}}$ applies to $\theta^{\mathrm{MAI}}_{\mathrm{O_2,air}}$, however, since oxygen purity is not a concern at this part of the process, for it will have to be purified later for hospital use, it is assumed that the fraction between $\theta^{\mathrm{MAI}}_{\mathrm{O_2,air}}$ and the mass fraction of O_2 in dry air is between 0.4 and 0.6.

Thus, $\theta^{\mathrm{MAI}}_{\mathrm{O_2,air}} = 0.231781 \times 0.4$ to $0.231781 \times 0.6 = 0.0927124$ to 0.1390686.

A.3 $\eta_{\text{el}}^{\text{m}}$

Stoichiometrically, $\frac{\text{M}_{H_2O}}{\text{M}_{H_2}} = 8.93669266$ is the the mass of water, in kilograms, necessary for each kilogram of hydrogen produced. Since LTD (2022) reported a consumption varying from 9.1 to 10 litters of water per kilogram of hydrogen, it is possible to calculate the $\eta_{\text{el}}^{\text{m}}$ as being the ratio between the fraction of the stoichiometric water requirement and the actual water consumption.

A.4 $\text{C}_{\text{el, min}}^{\text{CAPEX}}$

Equations 3.1 and 3.15 are sufficient to derive the following:

$$P_{el} = \frac{\eta_{el} \cdot Q_{el} \cdot (24)^{-1} \cdot 1000 \cdot \dot{m}_{\text{NH}_3}}{\eta_{\text{H-B}} \cdot \left(1 + \frac{\text{M}_{\text{N}_2}}{3\text{M}_{\text{H}_2}}\right)}. \tag{A.1}$$

Using the minimal value for $\dot{m}_{\text{NH}_3,min}$, it is possible to estimate $P_{el} = 1365.33$ kW. Thus, using 1851 \$/kW for the electrolyser, (RENAUDINEAU et al., 2025) $\text{C}_{\text{el, min}}^{\text{CAPEX}} = 2,527,230.46$

A.5 $\text{C}_{\text{H-B, min}}^{\text{CAPEX}}$

2020 (2020) report a Capex of \$32.11M - \$34.26M for a whole plant 20,000 tonnes of green ammonia per year and 2022 (2022) report that the H-B loop is usually responsible for 20-25% of the total Capex of a green ammonia plant. Therefore,

$$\text{C}_{\text{H-B, min}}^{\text{CAPEX}} = 0.25 \cdot 32.11 \times 10^6 \cdot \left(\frac{\dot{m}_{\text{NH}_3,min}}{54.757}\right)^k = 2.658\text{M US\$}_{2020} \tag{A.2}$$

To adjust for 2026 values, the Chemical Engineering Plant Cost Index (CEPCI) is used, which was 596.2 in 2020 and can be projected to be 842.0 in 2026 through a simple linear interpolation. (ECONOMIC..., 2024)

So $\text{C}_{\text{H-B, min}}^{\text{CAPEX}} = 3.7538\text{M US\$}_{t_0}$

A.6 Δ_{c_1,c_2}

LABREN — Laboratório de Modelagem e Estudos de Recursos Renováveis de Energia; CCST — Centro de Ciência do Sistema Terrestre; INPE — Instituto Nacional de Pesquisas Espaciais (2017) provides the latitude and longitude of each city in the dataset. Using these coordinates, it is possible to calculate the geodesical distance between each pair of cities.

A.7 $\mathrm{P}^{\mathrm{O}_2}$

MANHAS et al. (2024) have reported a price of 853 200 Rs./m^3 (which is approximately $335 US\$/$ tonne) and a cost for internal production of 342 311 Rs./m^3 (which is approximately $134 US\$/$ tonne) So the value used is the difference between the two, to account for the production costs.

A.8 $\mathrm{C}^{\mathrm{log}}$

BASTOS et al. (2024) have reported the costs for road transportation of liquid bulk trucks to be $16.61 \frac{R\$}{\text{Tonne}} + 0.21 \frac{R\$}{\text{Tonne}\cdot\text{km}} \cdot d$, with d being the distance traveled in kilometers. This would imply that $\mathrm{C}^{\mathrm{log}} = 0.21 + \frac{16.61}{d}$, taking an average distance of $d = 300$ km, $\mathrm{C}^{\mathrm{log}} \approx 0.265 \frac{R\$}{\text{Tonne}\cdot\text{km}}$. A very conservative estimate for $\mathrm{C}^{\mathrm{log}}$ was chosen, being $0.1 \frac{US\$}{\text{Tonne}\cdot\text{km}}$.